[illegible]

LA PRIMAVERA

GEOTHERMAL DEVELOPMENT PROJECT

IN UNITED MEXICAN STATES

FINAL REPORT

FEBRUARY, 1989

JAPAN INTERNATIONAL COOPERATION AGENCY

PREFACE

In response to a request from the Government of the United Mexican States, the Japanese Government decided to conduct a Preliminary Feasibility Study on La Primavera Geothermal Development Project and entrusted the study to the Japan International Cooperation Agency (JICA).

JICA sent to Mexico a study team headed by Mr. Hisayoshi Nakamura, Technical Adviser, Japan Metals & Chemicals Co., Ltd. from January 1985 to February 1989.

The team held discussions on the Project with concerned officials of the Government of Mexico and conducted field surveys in La Primavera area. After the team returned to Japan, further studies were made and the present report was prepared.

I hope that this report will contribute to the development of the Project and to the promotion of friendly relations between our two countries.

I wish to express my sincerest appreciation to concerned officials of the Government of Mexico for their close cooperation extended to the team.

February, 1989

Kensuke Yanagiya

Kensuke Yanagiya
President
Japan International Cooperation Agency

Geothermal Field of the Sierra La Primavera

Areal Photograph around the Sierra La Primavera

Main Geothermal Fields in Mexico

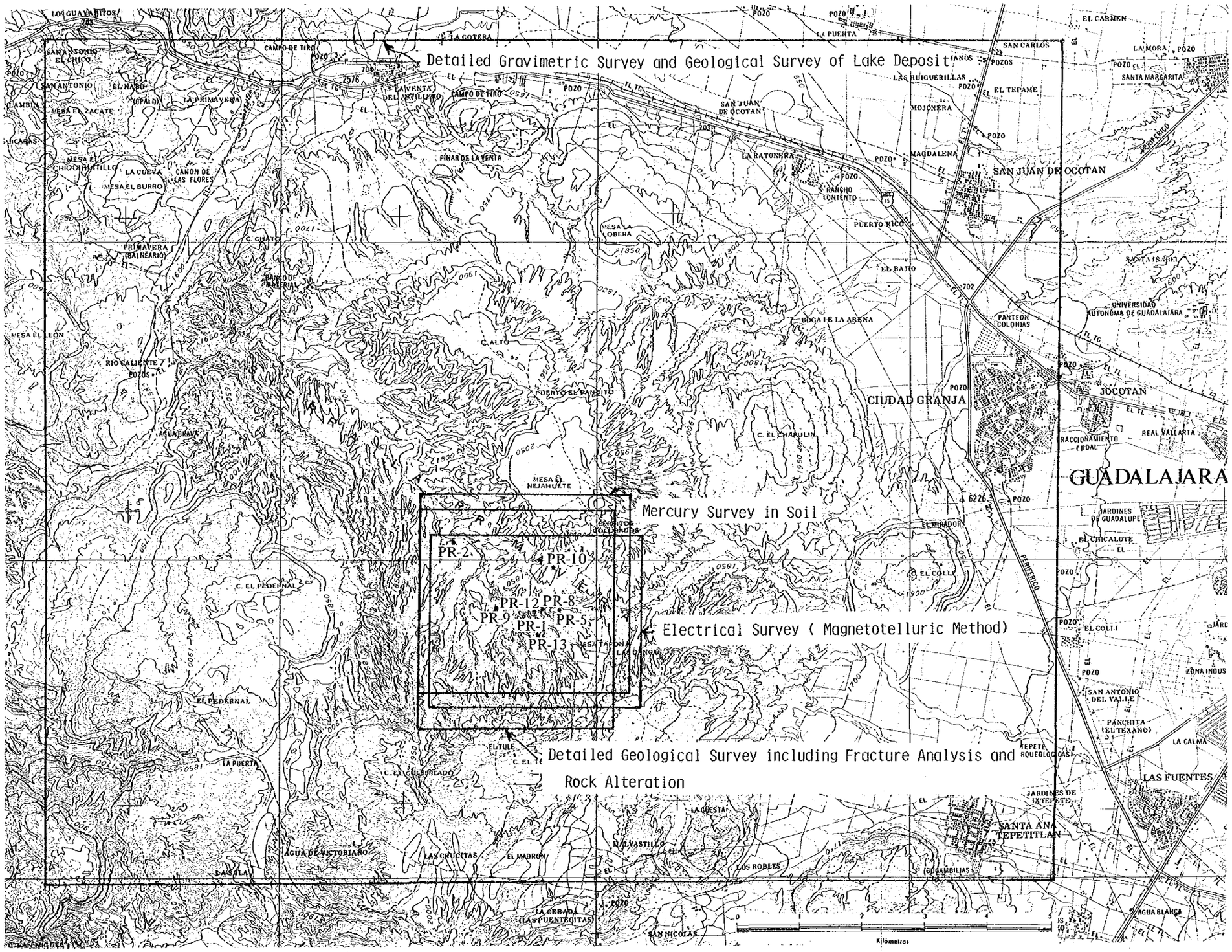

Locality Map of Survey Area

CONTENTS

III. GEOTHERMAL RESERVOIR EVALUATION

APPENDIX

List of Figs

List of Tables

List of Photographs

CONCLUSION

CONCLUSION

Progress of the Surveys Carried out for the Project

Japan International Cooperation Agency (JICA) has carried out Geothermal Development Project in La Primavera area in Mexico in cooperation with Comision Federal de Electricidad (C.F.E.) for four years since 1985. The purposes of the Project were to evaluate the geothermal reservoir and to estimate the possible capacity of geothermal power generation in La Primavera area, based on the results of geological, geochemical and geophysical surveys, of analysis of data obtained from the exploration wells drilled by C.F.E. and JICA and of well testing of the exploration wells.

In order to accomplish the purposes of the Project, the surveys were divided into two stages, the first and the second. In the first half of the first stage survey, geological, geochemical and geophysical (gravity and magneto-telluric (MT)) surveys and well testing of the exploration wells drilled by C.F.E. were carried out in 1985. Originally, it was planned that C.F.E. would drill three heat holes of 750m in depth as the survey in the second half of the first stage survey. However, because outline of the geothermal reservoir and distribution of underground temperature around the reservoir area became clear from the results of the surveys in the first half of the first stage survey and from analysis of existing data, it was agreed between C.F.E. and JICA that as the survey in the second half of the first stage survey, C.F.E. would drill an exploration well of 2,000m in depth for three heat holes to collect data necessary for analyzing the geothermal reservoir. The exploration well called PR-12 was drilled to a depth of 2,303m during the period from September, 1986 to January, 1987. Well testing of PR-12 was carried out in February, 1987 by JICA. By the change of work schedule made after drilling of PR-12, drilling of PR-12 and its well testing were included in the second stage survey. So, as the survey in the second half of the second stage survey following drilling of PR-12 and its well testing, drilling of an exploration well (PR-13) of 2,006.8m in depth was conducted by JICA in 1987. Well testing of PR-13 was carried out in 1988 which was the last year of the Project. Since all the field works were completed by the well testing of PR-13, after that, analyses of the data collected by the first and second stage surveys were carried out, and based on the results of analyses, Final Report which describes evaluation of the geothermal reservoir and possible capacity of the power generation in La Primavera area has been made. This is the outline of the progress of that Project.

Summary of the Results of the Surveys and Conclusion

Summary of the surveys carried out for four years and conclusion of the Project are shown as follows;

Geothermal reservoir in La Primavera area is characterized by development of the fractures trending from NW to SE in Cordilleran Volcanics existing at deeper than 1,000m from the surface.

These NW-SE fractures were reactivated by an uplift which occurred during the period of formation of the caldera, and the center of the uplift is considered to be existed around PR-1 and PR—8.

From the underground temperature distribution which was obtained from data on geochemical thermometer, fluid inclusion and temperature logging, it was found that the high temperature area is distributed near PR-1, PR-8 and PR-12. This fact suggests that the geothermal reservoir was formed in area where the uplift area overlapped with up-flow area with vertically developed fractures.

As to extent of the reservoir, it is estimated that it includes the points distributed near PR-10 on the north side, about 1km south of PR-8 on the south side, about 1km east of PR-1 on the east side and near PR-2 on the west side, therefore it occupies a rectangular area with about 2km in NW-SE and about 1.5km to the NE-SW.

Based on the above mentioned reservoir structure, reservoir evaluation by means of simulation was carried out. The simulator has such a capability that it can be used for multi-component two phase flow and for three-dimentional double-porosity grid model.

As horizontal division in the NW-SE direction with 4.8km was divided into 20 blocks and in the NE-SW direction, 4.2km into 18 blocks, and for the vertical division, geologic formation was divided into 5 layers, among which layer 3 was regarded as the main reservoir in this area. However, because a buffer zone was added to the outside of the above-mentiones area, the number of grids used for calculation reached 2.640 in total ($22 \times 20 \times 6$).

All boundaries with horizontal four directions and vertical two directions were regarded as an open system which means that fluid is supplied from the outside into the system with a state keeping initial temperature and pressure.

Initial temperature and pressure distribution was determined by the data on temperature recovery tests of each exploration well and pressure logging at static condition. Besides these, initial permeability (fracture permeability and matrix permeability), porosity, density, heat conductivity and specific heat were determined by the result of core analysis.

Since continuously measured data is not enough, matching to change of reservoir pressure in time which was measured at static condition and to change of fluidal temperature in time which was estimated from geochemical thermometer measured at the time of blowing out was carried out based on the data on flow rates obtained from production tests which were temporarily conducted.

Duration of matching was 2.589 days starting from May 20, 1981 and ending on June 30, 1988. Seven wells (PR-1, PR-2, PR-5, PR-8, PR-9 (layer 3). PR-9 (layer 4), PR-12, PR-13 (layer 3)) and eight items were taken for matching. Results obtained almost satisfactory.

In the above-mentioned matching, good agreement between measured values end calculated values could be obtained by modification of fracture permeability. The reason why fracture permeability was modified was that in most of the wells in this area, it was found that flashing occurrs outside of the wells, which means that fractures have poor permeability, then it was considered that adjustment of permeability would have an effect on matching. As the result, it was possible to make agreement between measured values and calculated values by lowering the values of permeability of fractures.

As the next stage, future prediction by simulation was carried out by using a model which was determined from the result of the above-mentioned matching. This was a prediction of behavior of the reservoir which occurrs when geothermal fluid is produced from the reservoir continuously with a state keeping fixed capacity of generation, namely flow rate of steam and

well-head pressure.

For this purpose, three cases, namely 50MW, 75MW and 100MW were selected for calculation. Necessary flow rate of steam for each output of generation was regarded as 500t/h, 750t/h and 1,000t/h respectively, and well-head pressure as 6.5ata. As to disposal of hot water produced with geothermal steam, injection into underground was not taken into consideration.

As the result of calculation, it was shown that judging from distribution of pressure and rate of water saturation after 20 years in fracture developed in layer 3 and layer 4 which are regarded as the main reservoir in this area, well-head pressure might be kept at a stable state although pressure and rate of water saturation would be decreased. However, in the case of 100MW, namely steam production of 1,000t/h, pressure and rate of water saturation would be decreased remarkably compared with other cases, which suggests that this amount of steam would be nearly the limit of that supplied from outside of the system.

On the other hand, in the case of 75MW, namely amount of steam production of 750t/h, pressure would be kept at about 6.8ata and rate of water saturation kept at about 35% for 20 years after power generation was put into operation, in the category of the grid including PR-9 where the most remarkable decrease of pressure and rate of water saturation would occur.

Therefore, judging from the results of future prediction by simulation, it is concluded that the possible capacity of power generation which can be operated at a stable state for long time is 75MW.

Proposal

This is the summary of the results of the surveys and conclusion of the Project showing the expected capacity of power generation is 75MW. However, this 75MW is possible capacity, so it is necessary to examine the following matters to determine what the best output is, before the power plant is constructed.

Among the existing exploration wells, the amount of steam has been measured in five wells, but not in two wells (PR-10 and PR-11). However, since it is estimated that the latter two wells will produce 40t/h of geothermal steam respectively, it is possible to produce 265t/h of steam in total at this moment, which corresponds to 26MW of power generation. Accordingly, it is expected that 50MW power generation is obtainable if 235t/h of steam can be produced more, and 75MW obtainable if 485t/h of steam be produced more.

Judging from the distribution of underground temperature, pressure and permeability, it is expected that 30 production wells may be drilled in this area. However, the problem is that how many production wells are needed to produce 235t/h or 485t/h of geothermal steam.

Since the number of the drilled production wells are deeply related with geothermal power generating cost, it must be said that a Feasibility Study including economy of power generation is indispensable for geothermal power development before capacity of a power plant is determined.

As mentioned above, there still remains unsolved problems at this moment, so it is proposed that the following surveys including the Feasibility Study will be made at the next stage.

In order to make the behavior of the reservoir clear, it is the best method to continue emission of geothermal fluid of all production wells of the same time for at least one year,

however, this method is uneconomical because of emission of steam, of which no utilization is made, so it may be impossible to carry out this method.

Another method which coveres the above-mentioned method by well-head generation is carried out in Los Azufres in Mexico at present. In this La Primavera area, if the same method is applied, 3 units (1 unit = 5MW), namely 15MW will be expected. The items are as follows: PR-9 for 1 unit, PR-1 + PR-12 for 1 unit and PR-11 + PR-13 for 1 unit. This method is useful for not only reducing idle hours of production wells before construction of a power plant is completed, but also for collecting data on behavior of the reservoir.

Parallel to the above-mentioned matter, it is necessary to study economical problems in the case of 50MW or 75MW power generation. In this subject, the number of needed production wells will be the most important factor.

Relating to this subject, it is proposed that in order to estimate the amount of geothermal steam produced from one well which will be drilled in future, two or three exploration wells are drilled in the area where distribution of underground temperature, pressure and permeability were shown in the survey. The reason why drilling of the exploration wells is needed is that, from the results of drilling and production tests of the exploration wells, it will become possible to estimate how much steam can be produced from production wells at the selected drilling site.

Accordingly, it is concluded that the best way to determine the capacity of a geothermal power plant to be constructed in the La Primavera area is to wait for the results of the proposed Feasibility Study and the examination and evaluation of production test in the newly drilled exploration wells.

I. INTRODUCTION

1. Background of the Project

United Mexican States is, in the same as Japan, situated on the Pan-Pacific Volcanic Belt and has many Quaternary volcanoes including active ones such as Parictin and El Chichonal and geothermal manifestations indicated by high temperature hotsprings and fumaroles which suggest wide distribution of geothermal resources with high energy potential. According to the long-term geothermal development plan by the Mexican Government, it is said that the aim of the plan is to save 11 million barrels of oil per year by geothermal power development of 60 billion KWh by 2000. Based on this plan, the Mexican Government has paid attention to development of geothermal resources which are expected to be reserved abundantly in the country, in order to promote reservation of oil resources and multiple utilization of other energy resources. As the result of execution of this plan, geothermal power plants have been installed in two areas, Cerro Prieto (620MW in 1989) and Los Azufres (80MW in 1989) by Comision Federal de Electricidad (CFE) as a principal development agency. At present, CFE is still promoting geothermal development projects in other geothermal areas.

Relating to this development plan, the Mexican Government requested the technical cooperation of geothermal development project to the Japanese Government in 1982. In accordance with this request from the Mexican Government, Japan International Cooperation Agency (JICA) carried out preliminary a survey to select a survey area for the Geothermal Development Project in 1983. From the result of the surveys carried out in the geothermal areas located on the central Mexican high land, it became clear that La Primavera is the most feasible area for geothermal development.

This Geothermal Development Project has been carried out by JICA in cooperation with CFE, as one of the international cooperation projects, to evaluate geothermal reservoir and estimate the possible capacity in La Primavera area.

2. Purposes of the Project

The purposes of the Project are to evaluate the goethermal reservoir and to estimate the possible capacity of power generation in La Primavera area, based on the results of geological geochemical and geophysical surveys and of analyses of the data obtained from the surveys.

3. Outline of the Survey Area

La Primavera volcanic area is located about 20km southwest of Guadarajara, the second biggest city in Mexico. The survey area is in a volcanic area, surrounded by caldera, 12km in a north-sourth direction and 11~12km in a east-west direction which was formed at the junction of three graben zones named Tepic-Chapala in the NW-SE, Chapala in the E-W and Colima in the N-S.

4. Outline of Progress of the Survey

The survey was divided into two stages, the first and the second.

In the first stage survey, geological, geochemical and geophysical (gravity and magneto-telluric) surveys and well-testing of the exploration wells drilled by CFE were carried out during the period from 1985 to 1986, to understand structure, extent and depth of the geothermal reservoir in this area.

Originally, it was planned that CFE would drill three heat holes of 750 m deep in the first stage survey. However since the outline of the geothermal reservoir and distribution of underground temperature around the reservoir area became clear from the results of the above-mentioned surveys and analysis of existing data, it was agreed between CFE and JICA to change the schedule as follows; CFE would drill an exploration well of 2,000 m deep to the collect data necessary for analysing the geothermal reservoir. The exploration well named PR-12 was drilled to a depth of 2,303 m during the period from September, 1986 to January, 1987. By the change of work schedule made after drilling of PR-12, drilling work of PR-12 was included in the second stage survey. Following drilling of PR-12, JICA exploration well, PR-13, was drilled to a depth of 2,006.8 m. Since all the field work was completed by drilling of PR-13 and its well-testing, after that, analyses of the data collected by the first and second stage surveys were carried out by means of simulation and based on the result of analyses, a Final Report describing the evaluation of the geothermal reservoir and possible capacity of power generation has been made.

5. Process and Period of the Survey

Process of the survey carried out during the period from 1984 to 1988 is shown in Tables-1 and 2.

6. Members of Study Team

Members of the study team are shown in Tables-3 and 4.

Table 1 Process of Survey

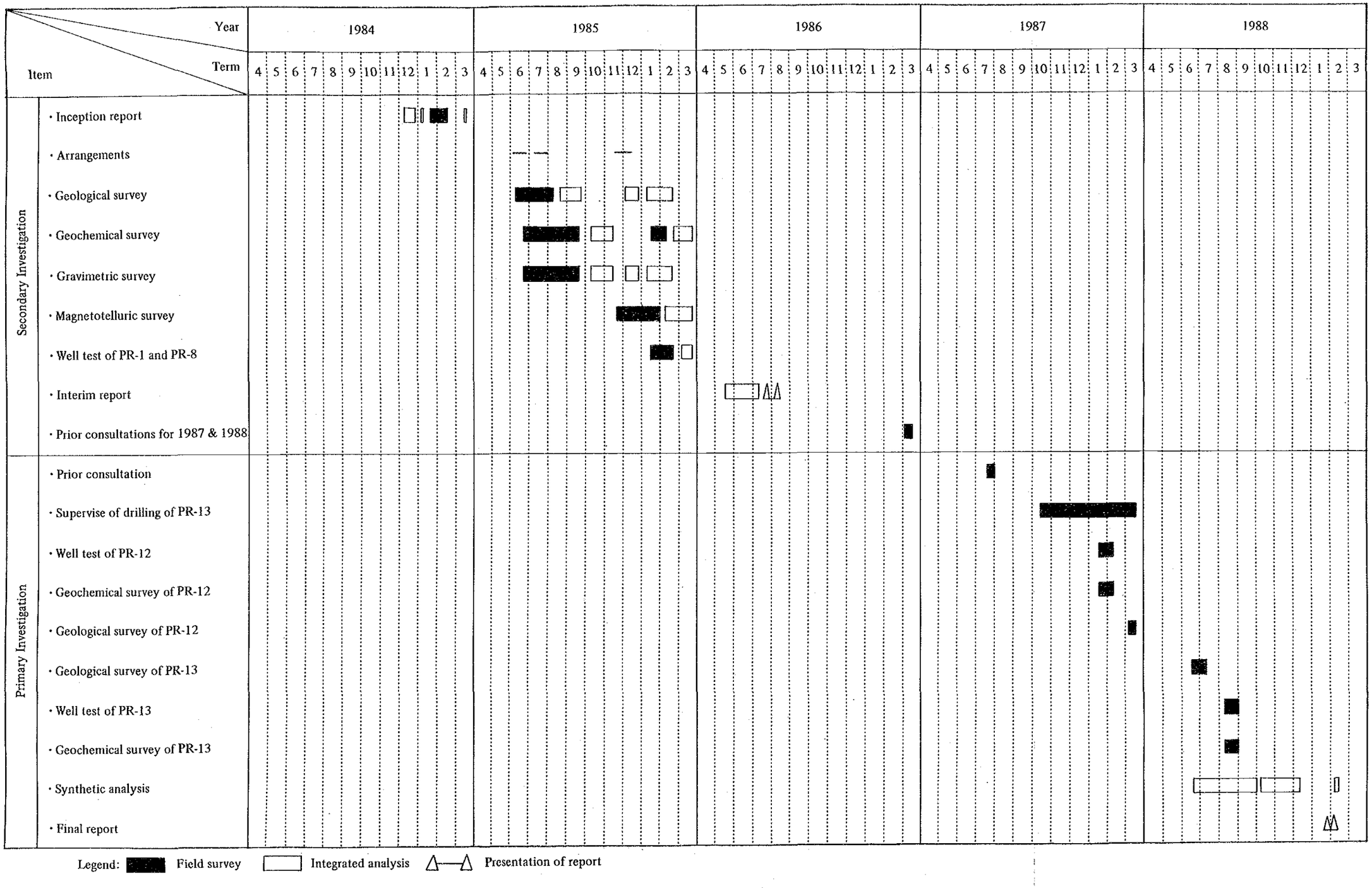

Table 2 Period of Survey

Item	Period	Field survey	Analysis
Primary Investigation	Inception report	From Jan. 20, 1985 to Feb. 17, 1985 29 days	From Dec. 20, 1984 to Jan. 18, 1985
	Collection of the data		From Feb. 19, 1985 to Mar. 20, 1985
	Geological survey	From Jun. 12, 1985 to Aug. 9, 1985 59 days	From Aug. 19, 1985 to Feb. 20, 1986
	Geochemical survey	From Jun. 24, 1985 to Sep. 20, 1985 89 days	From Oct. 11, 1985 to Mar. 20, 1986
	Gravity survey	From Jun. 24, 1985 to Sep. 20, 1985 89 days	From Oct. 11, 1985 to Feb. 20, 1985
	Electrical survey	From Dec. 27, 1985 to Jan. 31, 1986 66 days	From Feb. 3, 1986 to Mar. 20, 1986
	Interim report	From July 21, 1986 to Aug. 3, 1986 14 days	From Mar. 26, 1986 to July 8, 1986
	Collection of the data of PR-12	From Mar. 2, 1987 to Mar. 15, 1987 14 days	
Secondary Investigation	Prior consultation	From Jul. 20, 1987 Jul. 31, 1987 12 days	
	Supervise of drilling of PR-13	From Oct. 12, 1987 to Mar. 3, 1988 164 days	
	Well test and Geochemical survey of PR-12	From Jan. 20, 1988 to Feb. 12, 1988 24 days	
	Collection of the data of PR-12	From Mar. 9, 1988 to Mar. 23, 1988 15 days	
	Geological survey of PR-13	From Jun. 20, 1988 to Jul. 23, 1988 24 days	
	Well test and Geochemical survey of PR-13	From Aug. 8, 1988 to Aug. 31, 1988 24 days	
	Synthetic analysis for Final report	From Jun. 30, 1989 to Feb. 5, 1989 7 days	From Jun. 20, 1988 to Dec. 10, 1988 From Feb. 6, 1989 to Feb. 10, 1989

Table 3 Members of Study Team

Survey	Investigation	Name of member	Position
Leader	Primary ~ Secondary	Hisayoshi Nakamura	J.M.C
Vice Leader	Primary Primary ~ Secondary	Jiro Mihara Ko Sato	J.M.C J.M.C
Geological survey	Primary ~ Secondary " " Primary	Ko Sato Yoichi Muramatsu Tsutomu Oyama Akio Abe	J.M.C J.M.C N.M.C N.M.C
Geochemical survey	Primary ~ Secondary "	Yutaka Yoshida Kaichiro Kasai	J.M.C J.M.C
Gravimetric survey	Primary "	Shigeo Moribayashi Kunio Takahashi	N.E.D N.E.D
Magnetotelluric survey	Primary " "	Sumio Seki Haruya Nakata Nobuo Shinohara	J.M.C J.M.C J.M.C
Well test	Primary Primary ~ Secondary "	Jiro Mihara Yoshinobu Hirako Masasamu Oyanagi	J.M.C J.M.C N.E.C.
Drilling supervise	Secondary	Seiji Saito	J.M.C.

J.M.C : Japan Metals and Chemicals Co., Ltd.
N.M.C : Nittetsu Mining Consultants Co., Ltd.
N.E.D : Nikko Exploration and Development Co., Ltd.

Table 4 Members of Mexico- side Counterpart

MORELIA:	ING. HECTOR ALONSO ESPINOSA
	ING. ARTURO GONZALEZ SALAZAR
	ING. ANTONIO RAZO MONTIEL
	ING. RAFAEL MOLINAR CESEÑA
	ING. JAIME MARIO E. VACA SERRANO
	ING. JOSE PEREZYERA Y ZAPATA
	DR. JOSE LUIS QUIJANO LEON
	ING. ZENON CASARRUBIAS UNZUETA
	ING. SAUL VENEGAS SALGADO
	ING. FELIPE ARENAS GARCIA
	ING. ENRIQUE SAMANO SANCHEZ
	ING. CATARINO CADENAS TOVAR
	ING. MARCO ANTONIO TORRES RODRIGUEZ
	ING. MANUEL PINETTE GAONA
	TEC. MIGUEL LOPEZ DE NAVA
	ING. MOISES ZEPEDA PEÑA
	ING. AIDA LOPEZ HERNANDEZ
	DR. OSCAR CAMPOS E.
	ING. EMILIO BIGURRA P.
	ING. FERNANDO HERRERA B.
GUADALAJARA:	ING. LUIS C.A. GUTIERREZ NEGRIN
	ING. ROBERTO MACIEL FLORES
	ING. JAVIER VILLA MERLO
	ING. CESAR DANTE LUCIO
	ING. SERGIO SANCHEZ R.
	ING. RODOLFO BECERRA RAZO
	ING. OSCAR AQUINO MALDONADO
	ING. JOSE ROSAS ELGUERA
	ING. ARTURO ROSAS MARQUEZ
	TEC. MIGUEL CHACON FRANCO
	TEC. GUILLERMO MEDINA OROZCO
	SR. GUILLERMO BRISEÑO GARNICA
	SR. RENE BUCIO CAMBRON
	SR. ADALBERTO URIBE OJEDA

II. RESULTS OF SURVEY

1. Exploration at First Stage

1.1 Geological survey

1.1.1 Summary of geological survey

Geological survey includes two types of survey, namely field, and core and cuttings surveys. Fracture analysis, rock alteration survey and sedimentological analysis of the Lake deposits have been carried out in the field survey based on the making of a route map (1:2,000 in scale, see Appendix). Moreover, a regional geological survey of Tertiary System, which is the main reservoir in the geothermal manifestation area (this area) of Sierra La Primavera Caldera, has also been executed to make clear the structure and rock facies of the Tertiary System surrounding the Caldera.

Measurements were made on the physical properties of rock cores including density, porosity and thermal conductivity, and on the characteristics of cuttings such as magnetic susceptibility, chemical concentration of Hg and As, mineral identification by X-ray and fluid inclusion. The cores and cuttings were collected from existing wells (PR-1, 2, 5, 8 and RC-1).

The following are results of the geological survey in this area:

① The rock formation is composed of basement granitic rocks, the Cordilleran Volcanics, the Tala Tuff, the Cerritos Colorados Rhyolite, the Arroyo El Caracol Formation (Lake sediments) and the Mesa El Nejahuete Rhyolite in ascending order. The geothermal fluids are mainly stored in fractures developed within the lower Cordilleran Volcanics.

② The fracture analysis reveals that the NE-SW trending normal-slip faults are recognized at the surface and the upper Cordilleran Volcanics, and these faults were formed during the uplift after the Caldera collapse. Judging from the existence of tensional fracture and the restoration of the stress field, the center of uplift is situated around PR-1 and PR-8.

③ The surface rock alteration in this area is characterized by the NE-SW trending acidic alteration including Kaolinite and Alunite. The center of surface rock alteration is also located in the vicinity of PR-1 and PR-8. On the contrary, the altered minerals below 1,000 m in boreholes are represented by neutral or alkaline hydrothermal altered minerals including Chlorite, Calcite, Mixed-layer minerals.

④ The high Hg and As concentration in the cuttings reflects the fractures that occure during lost of circulation while drilling. The subsurface temperature profile drawn by the minimum homegenization of fluid inclusion in the cuttings shows that the geothermal fluids go up from the deeper part of PR-1 and PR-8 (that is, up-flow).

1.1.2 Surface geology in the geothermal manifestation area

The geological map (Fig. II.1-1) is edited by a route map (1:2,000 in scale) and a rock distribution map of CFE (1986), and covers about 7.5 km^2 (an extent of 2.5 km by 3 km) of the geothermal manifestation area situated the upstream of Arroyo El Caracol. Four major lithostratigraphic units are recognized in this area. They are the Tala Tuff, the Cerritos

Colorados Rhyolite, the Arroyo El Caracol Formation and the Mesa El Nejahuete Rhyolite in ascending order.

(1) Tala Tuff

About 95,000 years ago, pyroclastic flows erupted from the Sierra La Primavera and buried not only the inside of the Caldera but also the surrounding basings, covering some 700 km^2 (MAHOOD, 1980). These pyroclastic flows are named the Tala Tuff. The Tala Tuff crops out along the V-shaped vallies of Arroyo El Caracol and Arroyo Hondo in the geothermal manifestation area. The exposure of the lower part of the Tala Tuff occurs along the scarp just east of Rio Caliente (the downstream of Arroyo El Caracol).

The Tala Tuff is divided into more than 11 flow units, according to the present investigation and the well data, and ranges from 200 m to 700 m in total thickness. This fact means that the collapse of the Caldera did not occur at a single stroke, but that the eruption and the collapse proceeded simultaneously and repeatedly.

The Tala Tuff is characterized by dense welded tuff containing aphyric pumice in the middle part, and partial or non-welded tuff in both the upper and lower parts. Stratifications are observed in the non-welded parts containing surge-like sediments. Pumice fall is found at the bottom.

(2) Cerritos Colorados Rhyolite

In the northern half of this area, rhyolite lava is distributed under the lake sediments and above the Tala Tuff. The distribution of the lava is localized with 0 ~ 100 m in thickness, and is thicker in the East. The Rhyolite, named Cerritos Colorados Rhyolite, is older than that of Older Ring Domes (MAHOOD, 1980) and is originated from the lava dome which came up at the collapse center.

The Rhyolite is vesicular and glassy, and contains spherulite and obsidian in places. The flow structure is also well developed in the Rhyolite.

(3) Arroyo El Caracol Formation

The lake sediments are deposited on the Tala Tuff within the Caldera lake which was formed by the Caldera collapse. The lake sediments called Arroyo El Caracol Formation are mainly composed of sand, pumice tuff and gravel. They are divided into an upper part which shows remarkable lateral facies change and into a lower part which shows more lithoidal feature consisting of giant pumice, siltstone and sandstone. The thickness of the upper part attains a maximum of more than 50 meters and that of the lower part ranges from 5 meters to 30 meters. The existence of a partial paraconformity, observed in their boundary, suggests the emergence of the lake which is connected with the uplift and the lava dome forming. While, the lateral facies change indicates the volcanism during sedimentation on the lake and the movements associated with uplift and collapse.

The lower lake sediments consist of three units, namely siltstone dominant bed, giant pumice and alternating beds of pumiceous sandstone, siltstone and tuff, and intercalates conglomerate and subaqueous pumice fall. A 3-to 13-m-thick horizon of giant pumice blocks set in a diatomaceous ashy matrix were deposited over the entire caldera-lake. The blocks of

fully inflated pumice range from 0.2 to more than 6 m across, and are columnar-jointed in a crudely radial pattern. The pumice blocks tend to be large at the margins of the lake, but are smaller in diameter near the center of the lake. MAHOOD (1980) pointed out that the pumice blocks were originated from the central Rhyolite dome after the Caldera collapse, and floated to the margins of the lake.

The upper lake sediments are unconsolidated formations cónsisting of gravel, pumiceous sand, fine sand, diatomaceous silt, ash fall and various sedimentary facies. Fig II.1-2 shows the correlation of geological columns of this formation over the entire Sierra La Primavera Caldera.

(4) Mesa El Najahuete Rhyolite

The northern half of this area is covered by Rhyolite provided by Mesa El Nejahuete mountain. The mountatain is a composite dome of older ring dome (about 95,000 years ago) and younger ring dome (about 75,000 years ago). The Rhyolite exhibits vesicular, glassy, brecciate and obsidian facies.

1.1.3 Subsurface geology in the geothermal wells

Investigations were made on subsurface geology based upon a regional geological survey around the Sierra La Primavera Caldera which was carried out in 1985, and upon the data of CFE's original survey in the geothermal wells (SANCHEZ, 1988 MS).

(1) Basement granitic rocks

Granodiorite and Quartz-Monzonite are observed at 2,780 to 2,986 m in Well PR-9 drilled by CFE in 1985. They appear to be correlated to granitic rocks of the Mesozoic to the Neogene which are widely distributed in the Pacific Coast, southwest of this area.

Table II.1-1 and photo 1 show the microscopic observation of the granitic core collected from 2,985 to 2,986 m of PR-9 respectively. According to the result of the observation, the name of core is decided to be Biotite Granite.

(2) Cordilleran Volcanics

Volcanics ranging up to 2,500 meters in thickness are underlain by the above "basement". The Volcanics belong to "Sierra Madre Occidental" consisting of basaltic andesite, rhyolite lava or rhyolitic tuff. Lithic tuff at about 900 m in PR-1 is very similar to the partial welded pyroclastics of the Cordilleran Volcanics (CLOUGH, 1981) which is exposed in the north of Guadalajara City. Therefore, the lithic tuff probably belongs to the Cordilleran Volcanics (Fig. II.1-3).

The Volcanics are subdivided into the upper part composed mainly of lithic tuff and into the lower part consisting chiefly of andesite. The relationship between the upper and lower parts is an unconformity because of discordant showing in folding morphology (see geological profile, Figs. III.1-10~11).

CLOUGH (1981) pointed out that the Volcanics ranging in age from Miocene to Pliocene are associated with bimodal volcanic activity of rhyolite and baselt, and are divided into seven units. Andesite is so badly altered that pyroxene is replaced largely by zeolite, and that

plagiclase undergoes chloritization and epidotization. Table II.1-2 shows the chemical composition of representative andesites belonging to the Volcanics.

(3) Tala Tuff

Details of the Tala Tuff have already been described in separate part (1.1.2(1)). Figs. III.1-10 and III.1-11 illustrate that the Tala Tuff thickens to the north and thins to the south in this area.

1.1.4 Fracture survey and its analysis

(1) Fault

Fig. II.1-1 shows mappable faults based on a route map of 1:2,000 in scale. The NE-SW trending normal-separation faults are dominant and are cut by the NW-SE trending strike-slip faults. Besides, the reverse-separation fault is observed near PR-2. These fault systems appear to have been formed after dome up (several thousands years ago) since they cut the Mesa El Nejahuete Rhyolite. Table II.1-3 shows the description of faults developed in the geothermal manifestation area in view of their characteristics.

The NE-SW trending normal-separation faults are comparatively visible in the field because of forming conjugate set. However, opinions are diverse concerning the NW-SE trending faults because of their having lateral displacement. That is to say, it is difficult to judge these faults to be strike-slip unless the slicken-line of fault plane can be observed (Fig. II.1-4).

The subsurface faults and their genesis will be described in Chapter III-1.2.1.

(2) Restoration of stress field

Fault displacement observed in the surface indicates only the relative separation (Fig. II.1-4). Unless the real displacement (slip) is detected, it hardly seems possible to extend fractures observed in the surface into the deep subsurface without grasping the real characteristics of the fault. To make clear this problem, an attempt was made to take advantage of the restoration of stress field in determination of slip. Another attempt is to trace a displaced maker such as vein, key bed and so on.

Thus, the paleo-stress field was firstly restored from conjugate minor faults, slicken-line and tensional fractures which were observed at outcrops in the field (RAGAN, 1968). The results of principal stress anlysis are shown in Table II.1-4 and Figs. II.1-5 ~ 6, and are summarized as follows:

① The maximum principal compressive stress (σ_1) is approximately vertical, while the minimum principal compressive stress (σ_3) is nearly horizontal in the NW-SE direction in the geothermal manifestation area. It suggests that normal faults can develop easily to the NE-SW direction in this area.

② The above mentioned normal faults are complete normal-slip faults in rare cases, and almost all have a small lateral-slip component. There are a few oblique and lateral-slip faults in this area as given in Table II.1-4. Therefore, the presence of a strike-slip fault isn't doubtful.

③ The σ_3 of the Tala Tuff has the NE-SW direction. This stress trajectory is favorable for providing the NW-SE trending fault system.

④ The σ_3 is approximately perpendicular to the Caldera wall near the margins of Sierra La Primevera Caldera. This fact suggests that the restored paleo-stress field was formed by the Caldera collapse or uplift. However, it is acceptable that the stress field was formed by the uplift because the Caldera collapse proceeded on repeatedly and graduately.

Secondaly, in order to examine the relationship between the stress field and geological structure, an analysis was carried out on the making of a profile for each principle stress by the measurements of fractures and remnant magnetization of cores. The profile of NE-SW direction perpendicular to the σ_3 is shown in Fig. II.1-7, and the stress trajectories of the σ_2 and σ_3 by core measurements are shown in Fig. II.1-8.

The restoration of the stress field by core measurements has been made by the following methods:

Fractures with slickensides and veins are observed in the core taken from the wells. Since the core can not be collected along the oriented direction, a discussion about fracture orientation is generally impossible. However, in case of recent rocks which have nearly the same geomegnetic fields as that of the present time, the fracture orientation can be studied by means of measuring the remnant magnetization Accordingly, the real north has been determined by measuring the remnant magnetization using the astatic magnetometer after the detection of a temporary magnetic north about 8 cores in the field. The principal stress axis was restored from the observation of fracture orientation on the basis of this real north as shown in Table II.1-5.

The following results are obtained from Fig. II.1-7~8 and Table II.1-5:

① Looking at the bending from the σ_1 dip direction, anticlines and synclines in stress field can be drawn to the NE-SW direction. It means that the genesis of minor faults is connected with the uplift of the Caldera having the axis of NW-SE trend. An anticline in stress field is situated to the north of PR-1 and a syncline in stress field is located to the south of PR-9.

② The principal stress directions, except for 1,360 m of PR-2, are harmonized with those obtained on the surface. It suggests that fractures found from the surface geological survey would extend to the upper part of the Cordilleran Volcanics. However, it is questionable whether fractures can extend or not into the deeper part of the Cordilleran Volcanics.

③ Since an anticline in stress field restored from core measurements is also situated near PR-1, the place in and around PR-1 is a part of stress concentration formed by rock deformation, that is, an axis of anticlinal bending.

(3) Tensional fractures

Fig. II.1-9 shows tensional fracture distribution on the surface of the geothermal manifestation area. They are well developed between PR-1 and PR-8 conforming with an anticline in stress field restored from the paleo-stress analysis. This fact suggests that the tensional fractures were formed by a bending fold. Fig. II.1-10 indicates the orientation of tensional fractures in the Tala Tuff with random direction. Therefore, the fractures also include those of thermal stress origin which was caused by cooling stage of pyroclastics.

1.1.5 Surface alteration survey

Surface alteration survey was mainly carried out on the fumarole site in the geothermal manifestation area. Eighty two samples as representative altered rocks, preceded by the observation of fumarole and alteration characteristics in the site, have been analysed by means of powder X-ray diffraction method of identify alteration minerals. The alteration zones were defined at the same time. An example of observation of altered rocks is shown in Fig. II.1-11. The analyzing method of X-ray diffraction will be mentioned in 1.1.6.

The indentified alteration minerals are Quartz, Cristobalite, Tridymite, Kaolinite, Halloysite, Montmorillonite, Sericite, Alunite, Gibbsite and Pyrite. It is called the Kaolinite zone and the Alunite zone respectively where these two minerals recognize. The result of X-ray analysis is listed in Table II.1-6, and the collecting points of rock samples are present in Fig. II.1-12.

As shown in Fig. II.1-13, most of acidic alterations with fumarole belong to the Kaolinite zones, and are mainly distributed in the vicinity of PR-5 and PR-8 showing the NE-SW trend. The Alunite zones show very limited distributions enclosed by the Kaolinite zones about 150 m northwest of PR-8 and about 200 m east of PR-2.

1.1.6 Study on cores and cuttings

Measurements were made on the physical properties of rock cores including density, porosity and thermal conductivity, and on the characteristics of cuttings such as megnetic susceptibility, chemical concentration of Hg and As, mineral identification by X-ray and fluid inclusion. The cores and cuttings were collected from existing wells (PR-1, 2, 5, 8 and RC-1) at first stage.

The following is the method and results of measurements:

(1) Measurements of density, porosity and thermal conductivity of rock cores.

Twelve longitudinal-halfcut cores are collected from existing well, and are measured on density, porosity and thermal conductivity. The density is calculated from the relations of the weight of natural, dry and wet conditions.

The effective porosity is also based on the density values. The thermal conductivity was measured by the Box Probe method of thermal conductivity meter made in Showa Denko K.K (QTM-D_2 style) on test pieces who's surfaces were polished flat and smooth.

In Table II.1-7, the measuring values of density, effective porosity and thermal conductivity of cores are presented.

The following results are reached from the Table:

① The density of tuff tends to be lower than that of andesite, and the density of dense welded tuff is higher than that of partial welded tuff bearing no relation to depth or stratigraphic portion of tuff.

② The effective porosity of the core has a scattered value, but partial welding shows a tendency to large in effective porosity.

③ The thermal conductivity is proportional to the density. That is, high density rocks have good thermal conductivity.

(2) Magnetic susceptibility

When hot water penetrates into igneous rocks, Magnetite converts easily into Pyrite. Accordingly, under the assumption that magnetic susceptibility decreases with higher permeability, the magnetic susceptibility using cuttings collected from more than 1,000 m in depth were measured in wells PR-1, 2, 8 and RC-1. The cutting of which the average diameter was 2~3 mm included powdered irons originated during drilling. Therefore, the measurements, proceded by washing in water and drying, were done after freeing irons of cuttings as much as possible.

The magnetic susceptibility was measured employing a magnetic susceptibility meter made in Bison Co., (3101 A type) and using a cylindrical acrylic vessel with an inner diameter of 2.95 cm and a height of 8 cm. The magnetic susceptibility (X) was calculated from the following equation:

$$X \approx R \times \left(\frac{d}{d'} \right)^2 \times \frac{1}{\alpha'} \times 10^{-6} \quad (\text{emu/g})$$

Where,

R: indicated value of digital meter (emu/cm^3)
d : diameter of standard sample (cm)
d': inner diameter of vessel (cm)
α': apparent density of cuttings (g/cm^3)

The results shown in the columnar section of Figs. III.-1, 2 and 4 indicate a good conformity of the low susceptibility with lost circulation during drilling of well PR-8. However, in case of other wells, it is correlated with the lithology, for example, high susceptibility corresponds to fresh rock, while low susceptibility exists in the part of white clayey alteration zone.

(3) Chemical concentration of Hg and As in cuttings

Chemical analysis of Hg and As was carried out on the cuttings sampled from more than 1,000 m in wells PR-1, 2 and 8 to make clear the relationship between the subsurface fractures and the concentration of these elements as a geochemical logging. The Hg component was analyzed by the reducing gasification method using a mercury detector made in Hiranuma (HG-1 type), and the As component was analyzed by the same method using an atomic absorption spectrophotometer made in Shimazu (610-S type). Besides, the entire chemical composition of representative andesites have already been shown in Table II.1-2.

Figs. III.1-1~7 (comprehensive columnar sections of each well) show the results of Hg and As analyses which reflect the subsurface fractures. That is to say, the high concentration of Hg and As at 1,630 m in PR-1 corresponds to a lost circulation at about 1,620 m. Also, the high concentration of Hg and As at 1,490 m in PR-1 reflects probably a complete lost circulation at 1,445 m. In PR-2, the Hg concentration increases with the depth over about 1,950 mm and the As concentration over about 1,800 m. Such a concentration tendency increase is affected by continuous partial lost circulation which appeared at more than 1,822 m. Both Hg and As concentrations in PR-8 show a similar tendency having high peaks at 1,340 m, 1,460 m, 1,560 m, 1,610 ~ 1,690 m, 1,740 m and 1,810 ~ 1,850 m. These

correlate to the lost circulation at 1,328, 1,436, 1,564 ~ 1,569, 1,640 ~ 1,643, 1,752 and 1,790 ~ 1,793 respectively. Furthermore, the high concentration of As at about 1,130 m seems to reflect the lost circulation at about 1,100 m.

As mentioned above, the Hg and As concentrations in cuttings are useful for fracture detection in boreholes because these elements originated in volcanism and are concentrated and stored in the fractures.

(4) X-ray diffraction analysis of cuttings

A total of 100 samples were selected out from the cuttings from below 1,000 m in wells PR-1, 2 and 8 by reference to the microscopic study of CFE, and were submited to X-ray diffraction analysis.

The X-ray diffraction was analyzed by powder of both bulk and hydraulic elutriation. The samples were bent by diffraction for powder of ethylen glycol, hydrochloric acid and heating (at 100°C) treatments as occasion demanded to identify the clay minerals. The X-ray diffractometer and diffractive conditions were as follows:

Diffractometer	:	Geigerflex RADTIIIA made in Rigaku Co.,
X-ray tube	:	Cu
Filter	:	Ni or monochrometer
Voltage and electric current	:	40 kV, 30 mA
Counter	:	Sintillation counter
Scale	:	1,000 ~ 8,000 cps
Time constant	:	1 sec.
Slit system	:	1° – 0.15 mm – 1°
Scanning degree (2θ)	:	2 ~ 40° (bulk sample)
		2 ~ 15° (hydraulic elutriation and other treatments)
Scanning velocity	:	2°/min (back sample)
		1°/min (hydraulic elutriation)
Recorder velocity	:	2 cm/min

The results of X-ray analysis are shown in Figs. III.1-1~7. The identified clay minerals are Montmorillonite, Mixed-layer mineral of Sericite and Montmorillonite, Mixed-layer minerals of Chlorite and Montmorillonite, Chlorite, Sericite and Talc. The others are Quartz, Cristobalite, Calcite, Dolomite, Siderite, Clinoptilolite, Wairakite, Heulandite and Pyrite.

The surface rock alteration in the geothermal manifestation area is characterized by the acidic alteration including mainly Kaolinite accompanied with fumaroles. On the contrary, the altered minerals below 1,000 m in boreholes are represented by neutral or alkaline hydrothermal altered minerals including Montmorillonite, Chlorite, Sericite, Mixed layer minerals, Calcite and Dolomite. The Wairakite recognized at 1,830 m of PR-8 indicates the alteration under his temperature in this site, although difficulties were found in the drawing of a subsurface temperature profile based on the distribution of identified altered minerals. Moreover, the presence of Epidote observed by microscopic study also shows the high temperature at the subsurface. However, the Epidote was not identified by X-ray diffraction because of the weakness and overlapping of diffraction.

(5) Fluid inclusion study

Quartz, Calcite and Amkerite were selected out from cuttings in PR-1, PR-2, PR-5, PR-8 and RC-1, because these minerals are suitable to determine the homogenization temperature of fluid inclusion. The results of the measurements using heating microscope for each well are as follows (see Figs. III.1-1~7):

PR-1: The minimum homogenization temperature at the depth less than 1,100 m is nearly the same as the static downhole temperature (Standing time = 408 hr.). Whereas the homogenization temperature becomes lower by 42~45°C than downhole temperature indicating a value of 260~284°C as the minimum homogenization temperature at the depth more than 1,500 m. A coexistence of both gaseous inclusions and liquid inclusions was observed, resulting in an assumption that a part of geothermal fluids produced a boiling in the initiation phase of inclusions.

PR-2: The minimum homogenization temperature increases with the depth gradually from 118°C at 680 m to 150°C at 1,780 m. However, the increase in temperature becomes abrupt at a depth more than 1,780 m, showing 240°C at 1,985 m near the bottom.

PR-5: Since cuttings were missing at a depth more than 895 m, the measurement was thus carried out up to this depth. The minimum homogenization temperature increased drastically from 104°C at 350 m to 144°C at 580 m. Then, some decreases in temperature were observed up to 750 m, followed by a steep increase from 750 m to 800 m.

PR-8: The downhole temperature decrease was observed at a depth of about 1,800 m where is a main feed point. Except for this depth and 1,250 m, both borehole temperature and minimum homegenization temperature curves show the same pattern. Further, the both values are fairly similar at 1,630 m. It is concluded from the above facts that the distribution of the minimum homogenization temperature would be close to that of subsurface temperature before drilling. The highest value of the minimum homogenization temperature is 292°C at 1,790 m. It is assumed, as in the case of PR-1, that this well also encountered a partial boiling of the geothermal fluid in the initiation phase in inclusions.

RC-1: The minimum homogenization temperature increases gradually from 78°C at 890 m to 122°C at 1,855 m. The highest value amounts only 122°C at 1,855 m which indicates very low temperature in comparison with the temperature of other wells.

The temperature profile by the minimum homogenization of fluid inclusion will be illustrated in a separate chapter (Chapter III) which deals with the measurement results of other wells in addition to the above mentioned five wells. In any case, it is inferred that the geothermal fluids in this area upflow along the deep-seated fractures around PR-1 and PR-8.

Representative photographs by microscopic observation of fluid inclusion are given in photo 2.

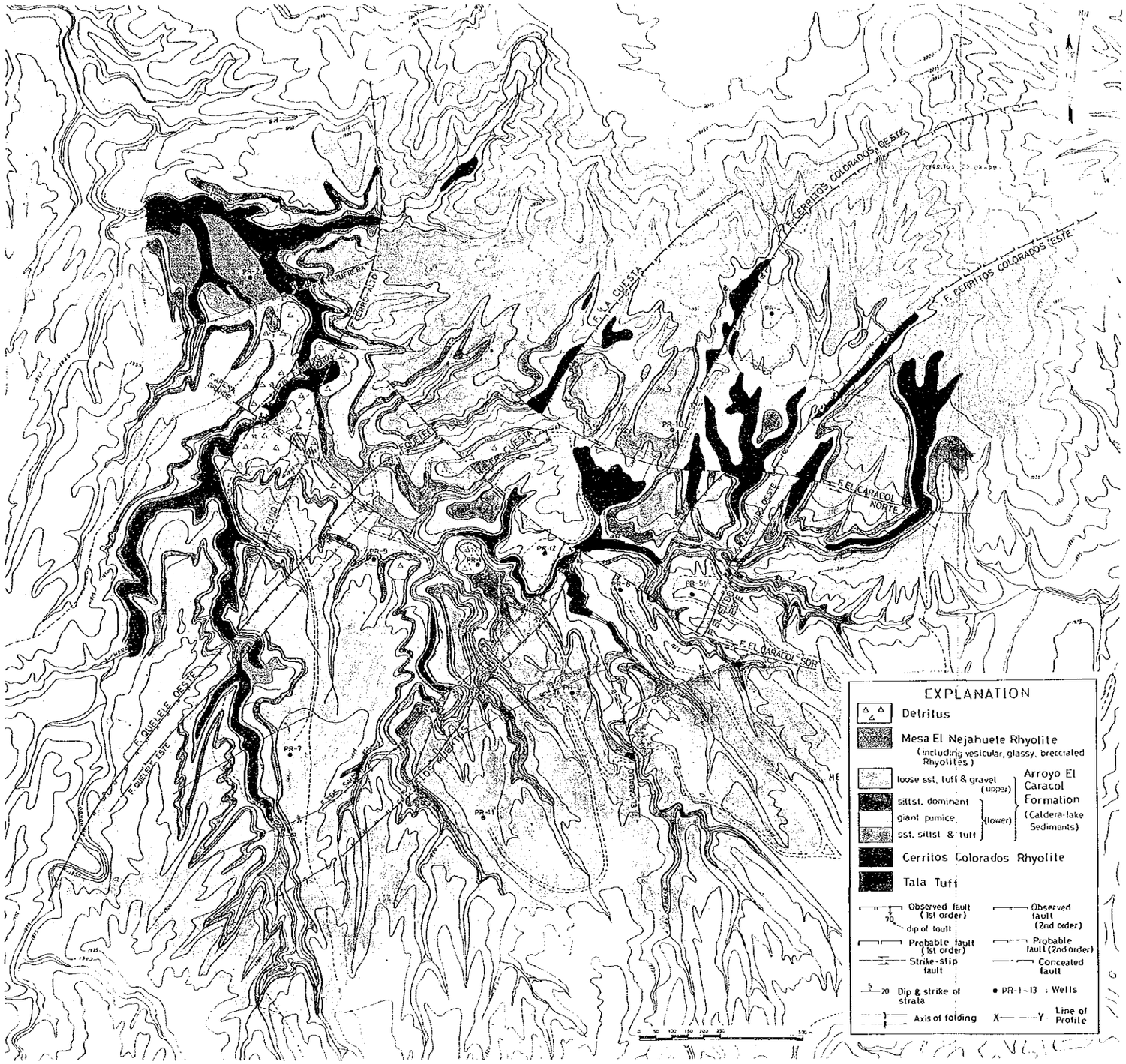

Fig. II. 1-1 Geological Map

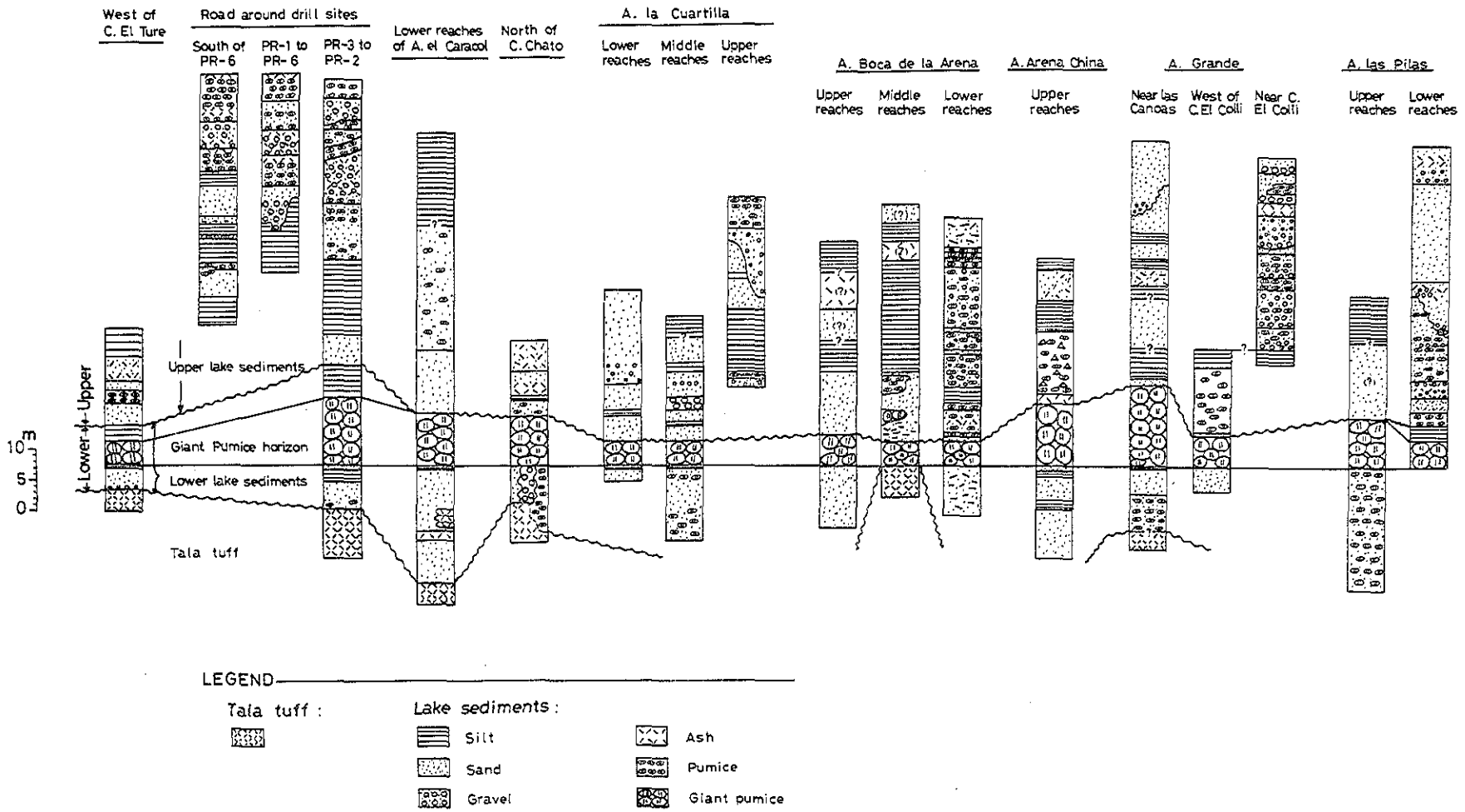

Fig. II. 1-2 Correlation and Stratigraphical Columns of the Arroyo El Caracol Formation

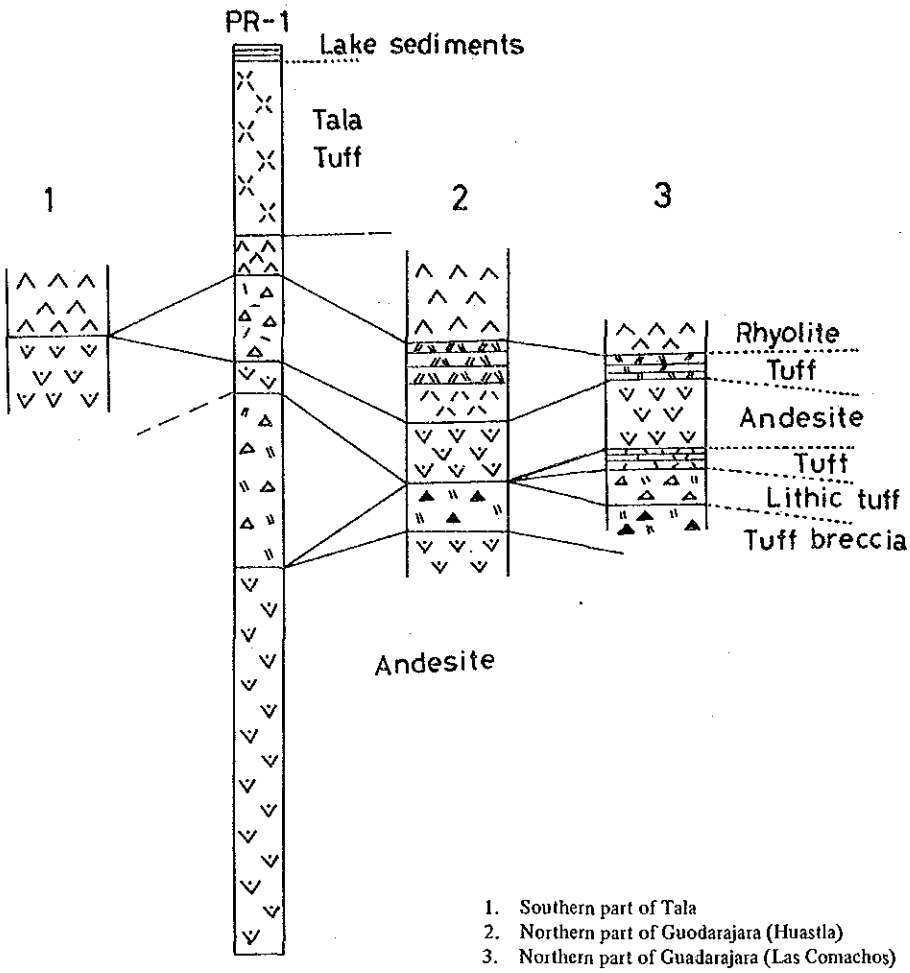

Fig. II.1-3 Correlation and Columns of the Cordilleran Volcanics

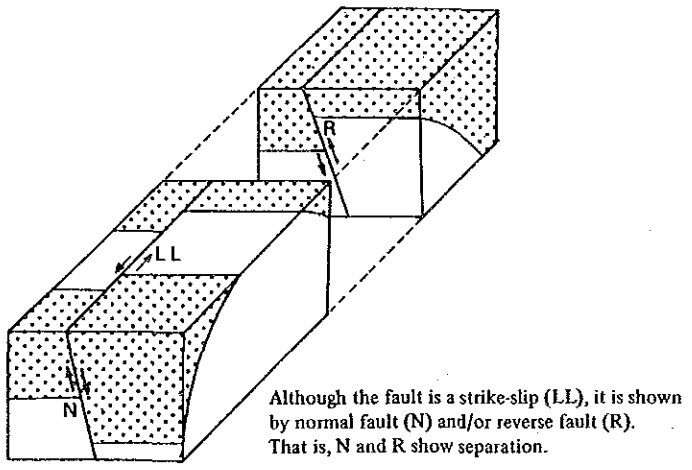

Fig. II. 1-4 Schematic Diagram of Strike-ship Fault

Table II. 1-1 Microscopic Characteristics of Biotite Granite

1) Sample No. 2
2) Rock Name Biotite Granite
3) Locality Well PR-9 Core (depth 2,985 ~ 2,986 m)
4) Microscopic characteristics

Texture		Granitic	
		Phenocryst	Groundmass
Mineralogy	plagioclase	1 ~ 3 mm in size, rectangular, euhedral ~ subhedral, albite and carlsbad twinning. Some plagioclases partly alters to sericite and chlorite (10 μm ± in size).	
	biotite	0.8 to 1.2 mm is size, subhedral, tabular, pale green to green pleochroism. Most characteristically biotite alters to iron-chlorite.	
	quartz	0.5 to 1 mm is size, anhedral	
	K-feldspar	0.5 to 1 mm in size, anhedral	
	opaque mineral	0.1 to 0.5 mm in size, granular, euhedral ~ subhedral.	
	zircon	0.1 to 0.15 mm in size, euhedral ~ anhedral.	
	apatite	0.05 to 0.2 mm, euhedral, rare mineral rectangular.	
	rutile	very rare, 10 to 30 μm ± in size.	
Alteration		Most mafic minerals alter to chlorite and epidote. Calcite veinlet up to 2 mm in width is developed in the granite. Epidotigation is very strong.	

Table II. 1-2 Chemical Analysis of Cutting Samples

Sample locality		PR-1, 1,540 m	PR-8, 1,160 m	PR-8, 1,710 m
Rock name		Andesite	Andesite	Basaltic andesite
Chemical composition	SiO_2 (%)	57.6	59.6	49.9
	TiO_2	1.33	1.60	1.62
	Al_2O_3	15.9	15.5	16.3
	Fe_2O_3	4.15	4.06	4.16
	FeO	3.03	2.92	5.17
	MnO	0.12	0.12	0.16
	MgO	2.48	1.52	5.21
	CaO	5.05	4.49	8.25
	Na_2O	3.93	4.25	2.55
	K_2O	2.83	2.34	0.37
	P_2O_5	0.25	0.38	0.28
	H_2O (+)	1.77	1.73	3.37
	H_2O (–)	0.26	0.16	0.28
	CO_2	1.00	0.75	2.34
	S	0.05	0.04	<0.01
	Sum	99.75	99.46	99.96
CIPW Norm classification	Q (%)	12.80	17.16	13.72
	C	0.11	0.46	2.80
	or	16.72	13.83	2.19
	ab	33.25	35.96	21.58
	an	17.10	15.05	24.30
	en } hy	6.18	3.79	12.98
	fs } hy	0.06	–	3.66
	mt	6.02	5.02	6.03
	hm	–	0.60	–
	il	2.53	3.04	3.08
	ap	0.58	0.88	0.65
	(cc)	(2.27)	(1.71)	(5.32)
	pr	0.09	0.07	<0.02
	sum	97.71	97.57	96.31
	Sum of Salic mineral	79.98	82.46	64.59
	Sum of Femic mineral	15.46	13.40	26.40
	D.I. (Q + or + ab)	62.77	66.95	37.49

Table II. 1-3 Description of Faults in Geothermal Area

Category of fault	Magnitude of fault	Name of fault	Dip & strike of fault	Fault character	Remarks
NE-SW trending faults	1st Order	Quelele Oeste fault	N34E 78E ≀ N64E 64E	Normal-separation fault	Same fault, probable in the northern part
		La Cuesta fault	N63E 66E	Normal-separation fault	
		Embalse fault	N30E 70E ≀ N35E 80E	Normal-separation fault	Same fault, obscured in the southern part
		Cerritos Colorados Oeste fault	Strike of NNE ~ NE	Probable fault, east side down	
		Los Muertos fault	N26E 76W ≀ N58E 90	Normal-separation fault	Same fault, coincides with axis of an anticline in the southern part
		El Ejido Este fault	N26E 77W	Normal-separation fault	
		Cerritos Colorados Este fault	Strike of NE	Probable fault, west side down	
	2nd order	Quelele Este fault	Strike of N30E	Probable fault, west side down	Conjugate set with Quelele Oeste
		Los Sanchez fault	N30E 82E ≀ N50E 82E	Normal-separation fault	Conjugate set with Los Muertos
		El Ejido Oeste fault	N29E 88E	Normal-separation fault	Conjugate set with El Ejido Este
NW-SE trending faults	1st Order	El Caracol Norte fault	Strile of WNW	Probable left-lateral-slip fault	Probable high angle north dip
		El Caracol Sur fault	Strike of NW ~ WNW	Probable right-lateral-slip fault	
		Arena Grande fault	N83W 83N	Probable left-lateral-slip fault	
Others	2nd Order	La Azufrera fault	N60E 70N	Normal-separation fault	
		Arroyo Hondo fault	N40E 72N	Normal-separation fault	
		Pino fault	N20E 81E	Normal-separation fault	Same fault
		Cerro Alto fault	NS trending	Probable fault, east side down	
		Barrancas fault	N60E 77N	Normal-separation fault	Same fault
		Canoas fault	N70E 84N	Normal-separation fault	
		El Caballo fault	N20W vertical	Probable Right-lateral-slip fault	

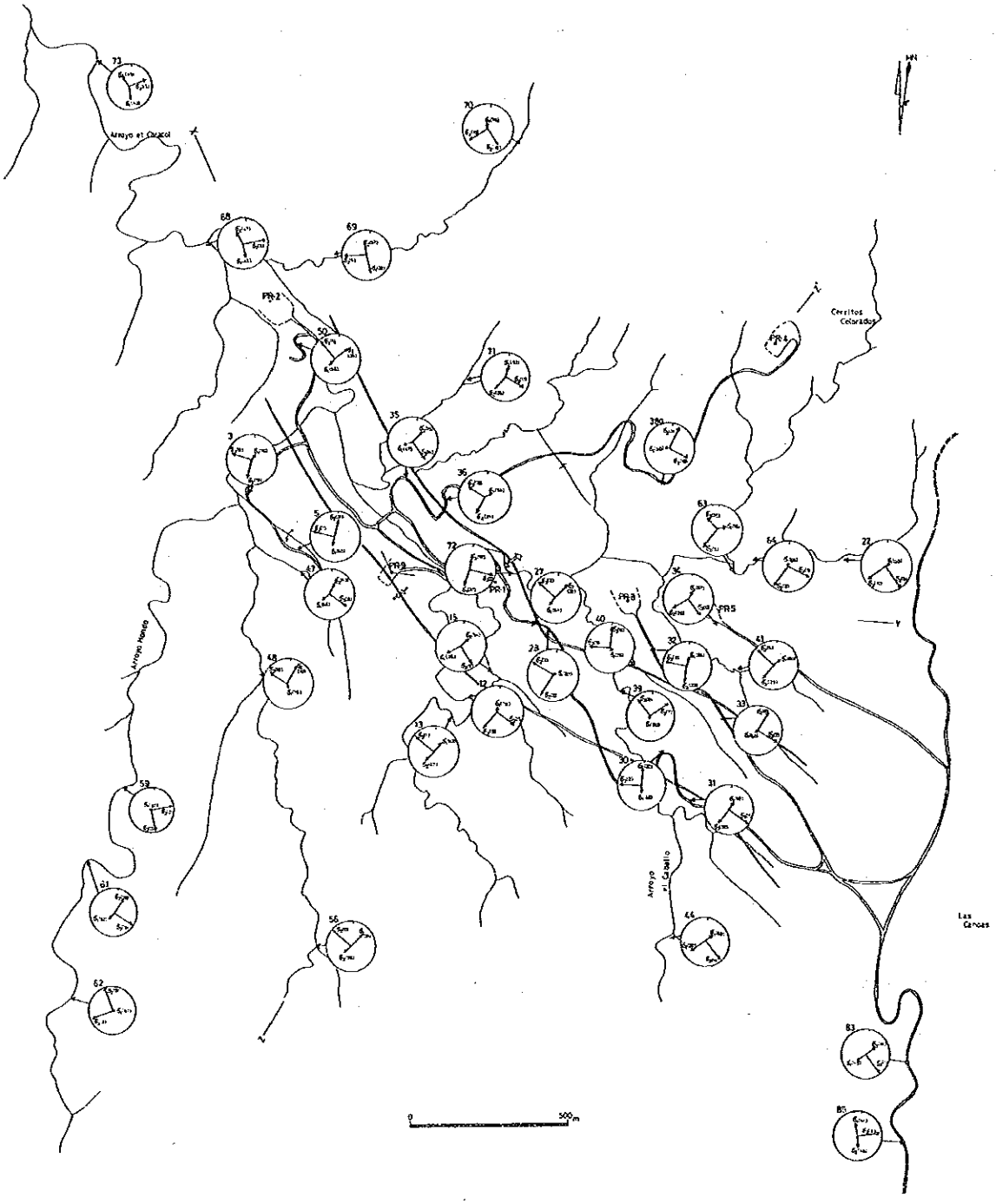

Fig. II. 1-5 Principal Stress and Its Trajectory in Caldera Area

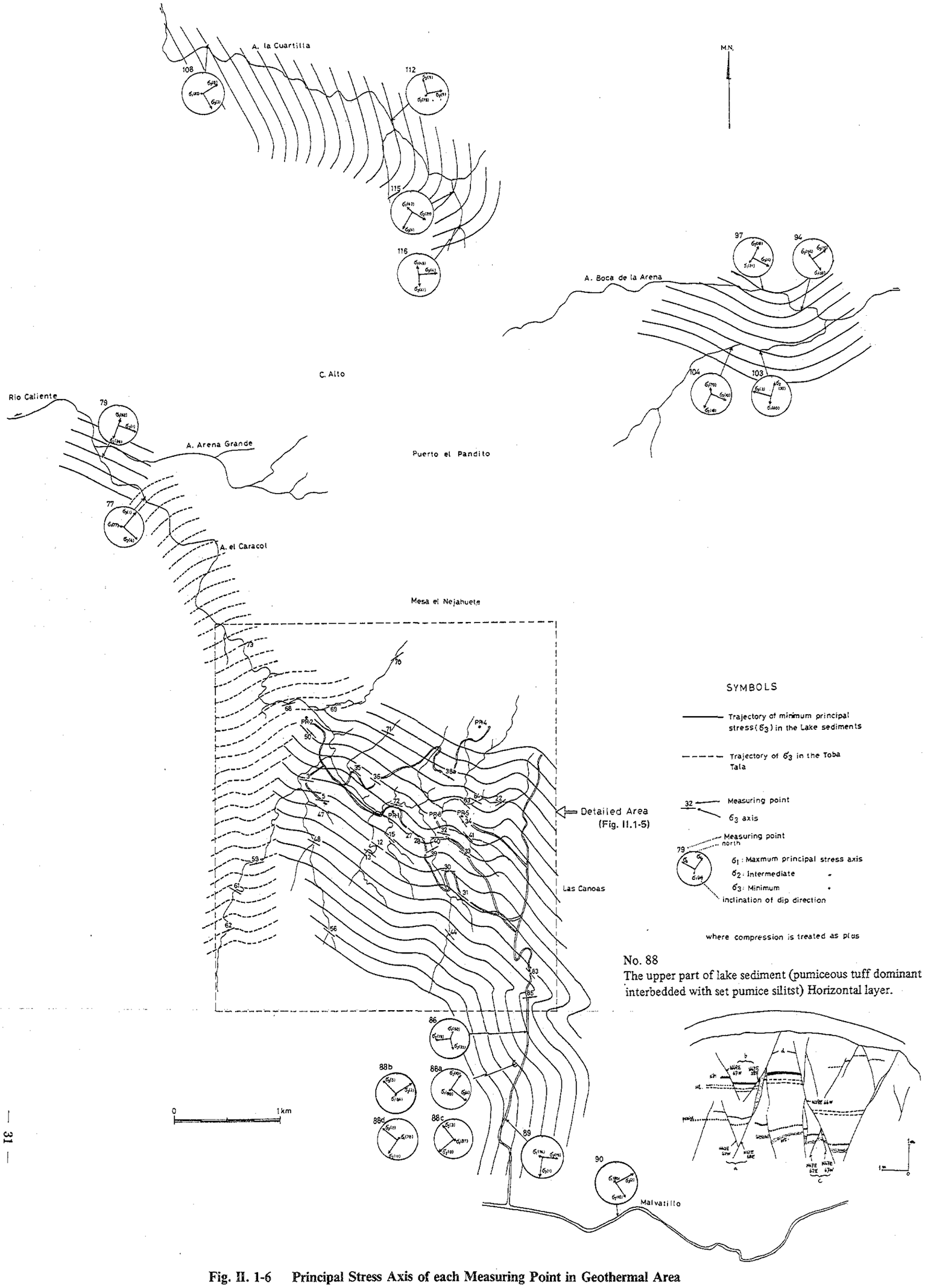

Fig. II. 1-6 Principal Stress Axis of each Measuring Point in Geothermal Area

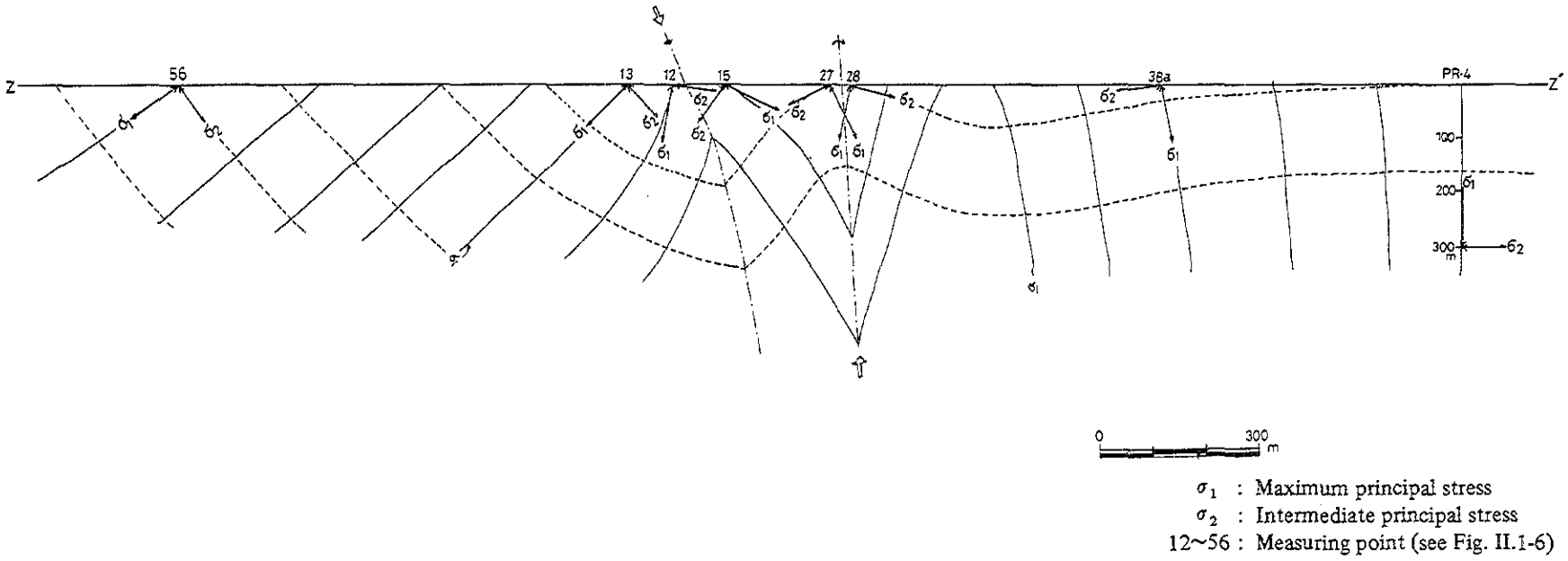

Fig. II. 1-7 Profile of Principal Stress Trajectory along NE-SW Section in Geothermal Area

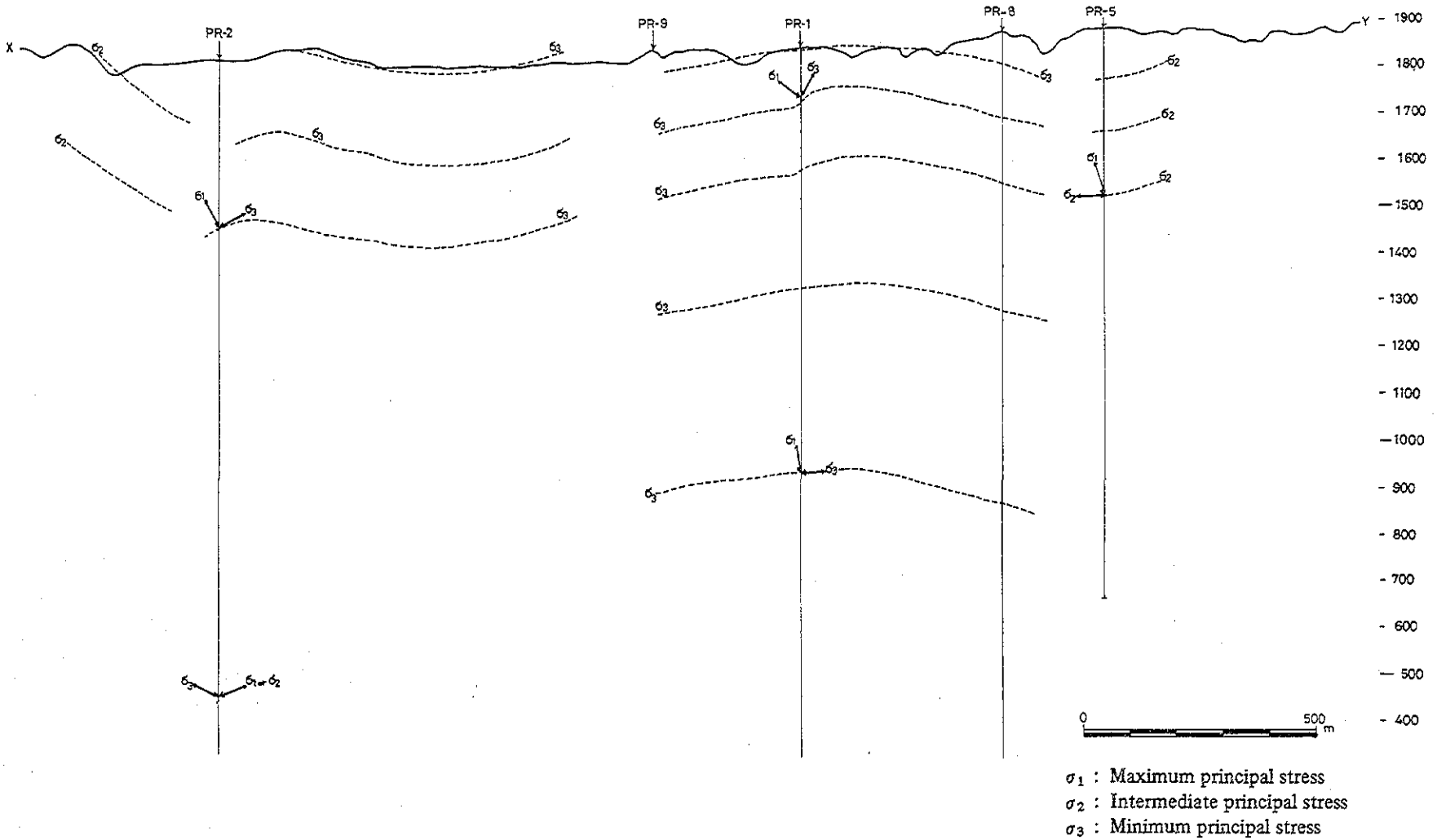

Fig. II. 1-8 Stress Trajectory Restored by Remnant Magnitization and Fracture Orientation of Cores

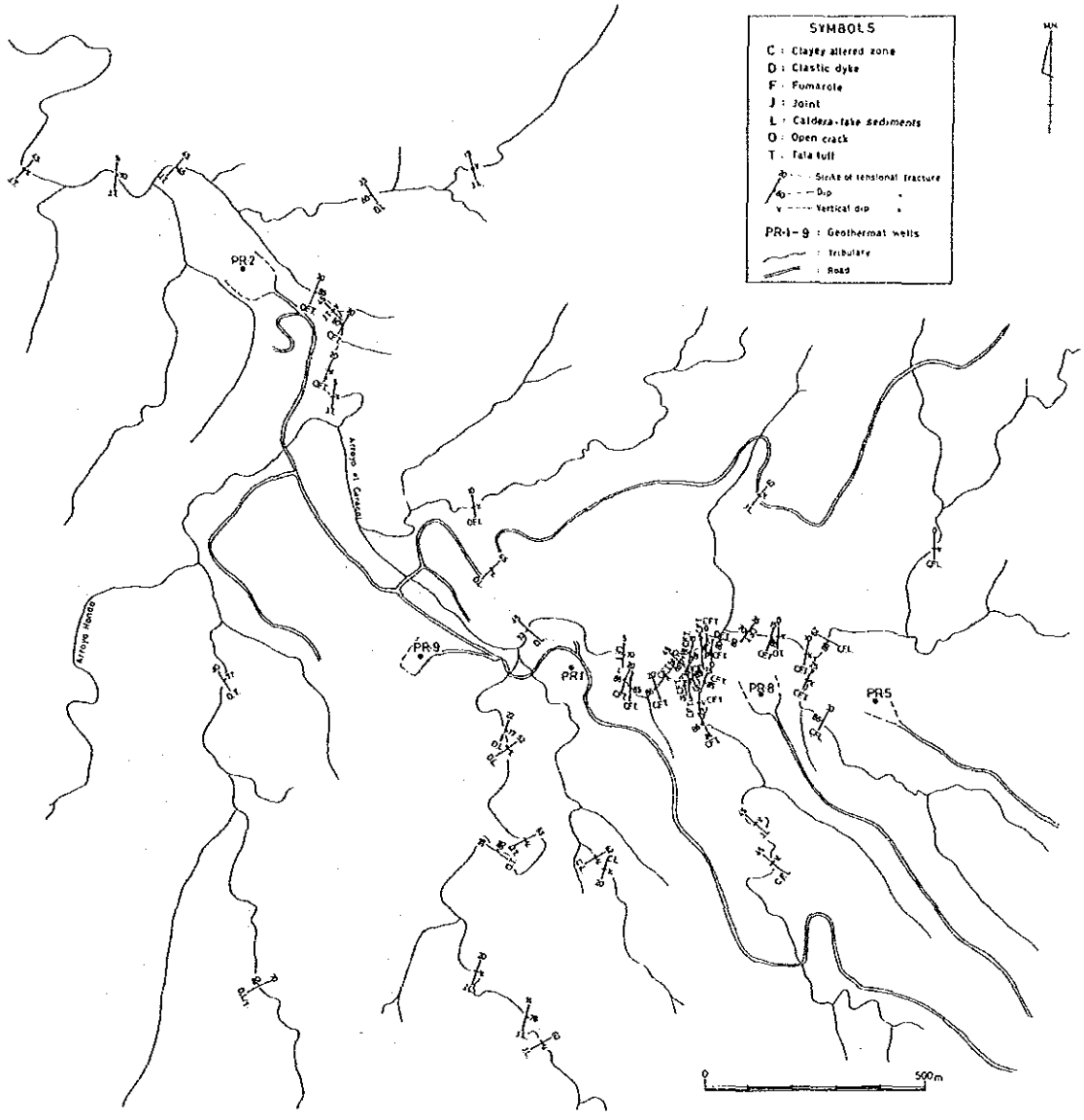

Fig. II. 1-9 Map Showing Tensional Fracture in Geothermal Area

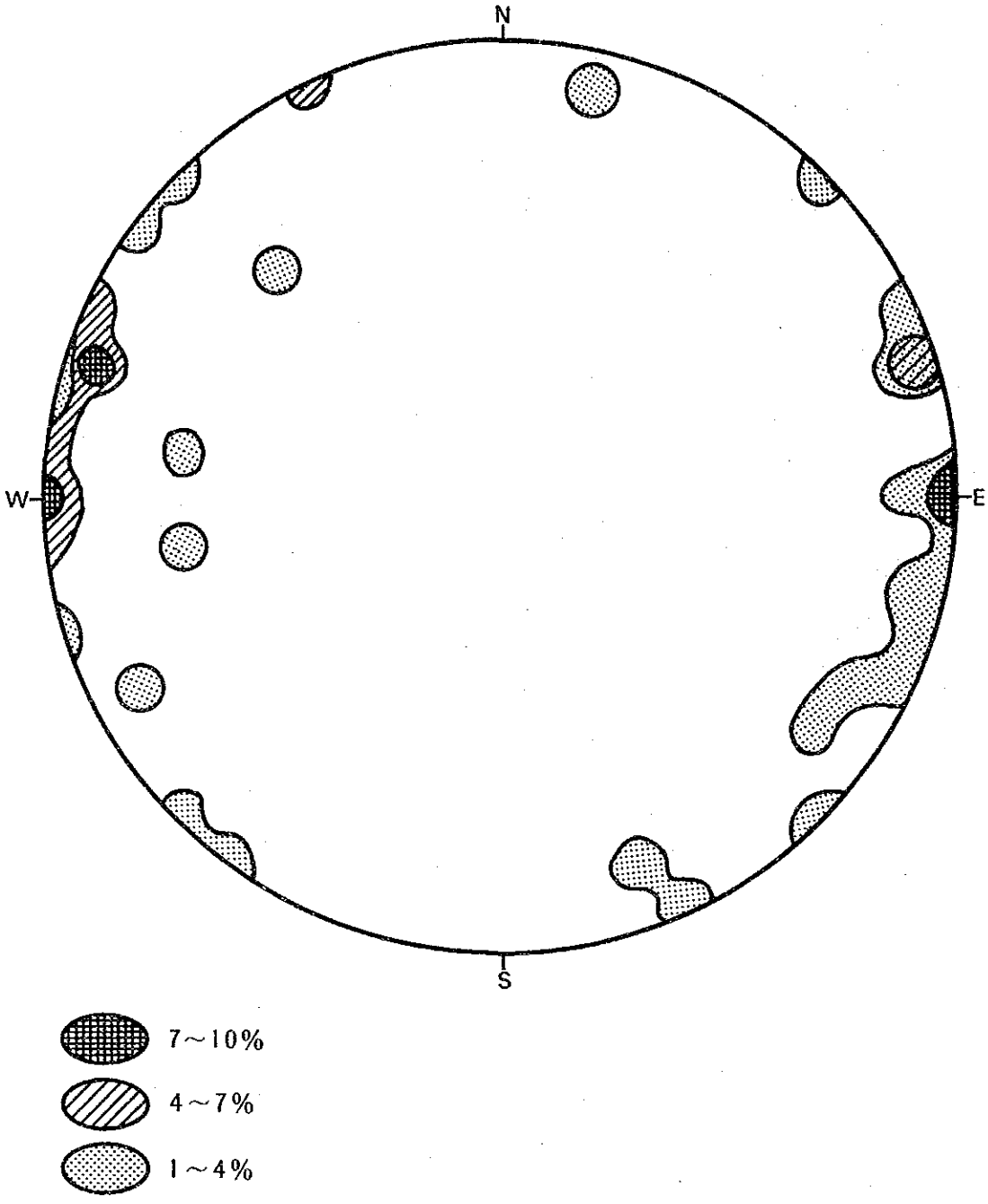

Fig. II. 1-10 Orientation of Tensional Fracture in the Tala Tuff at 35 Measuring Points

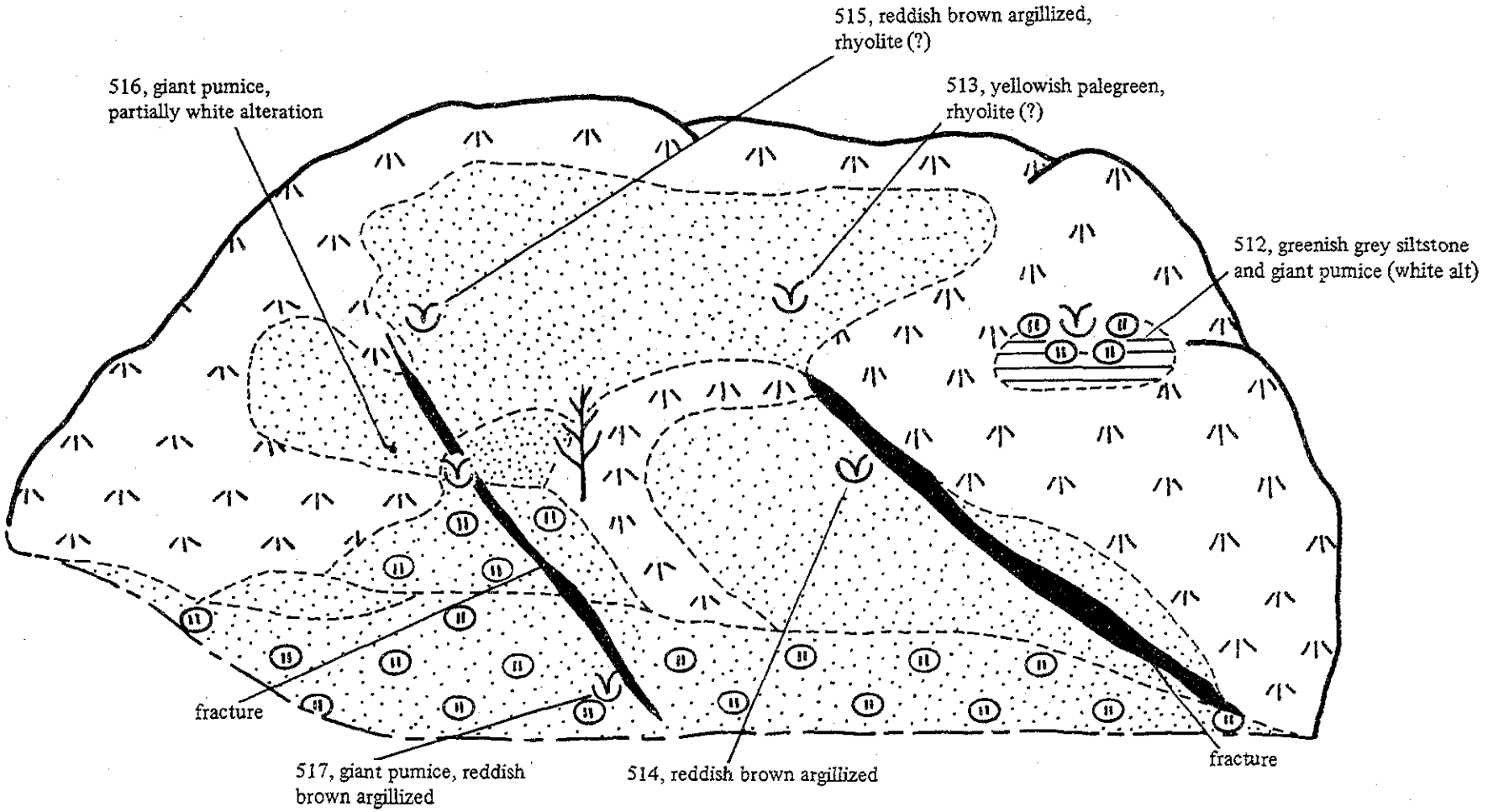

Fig. II. 1-11 An Example of Surface Outcrop of Altered Rocks

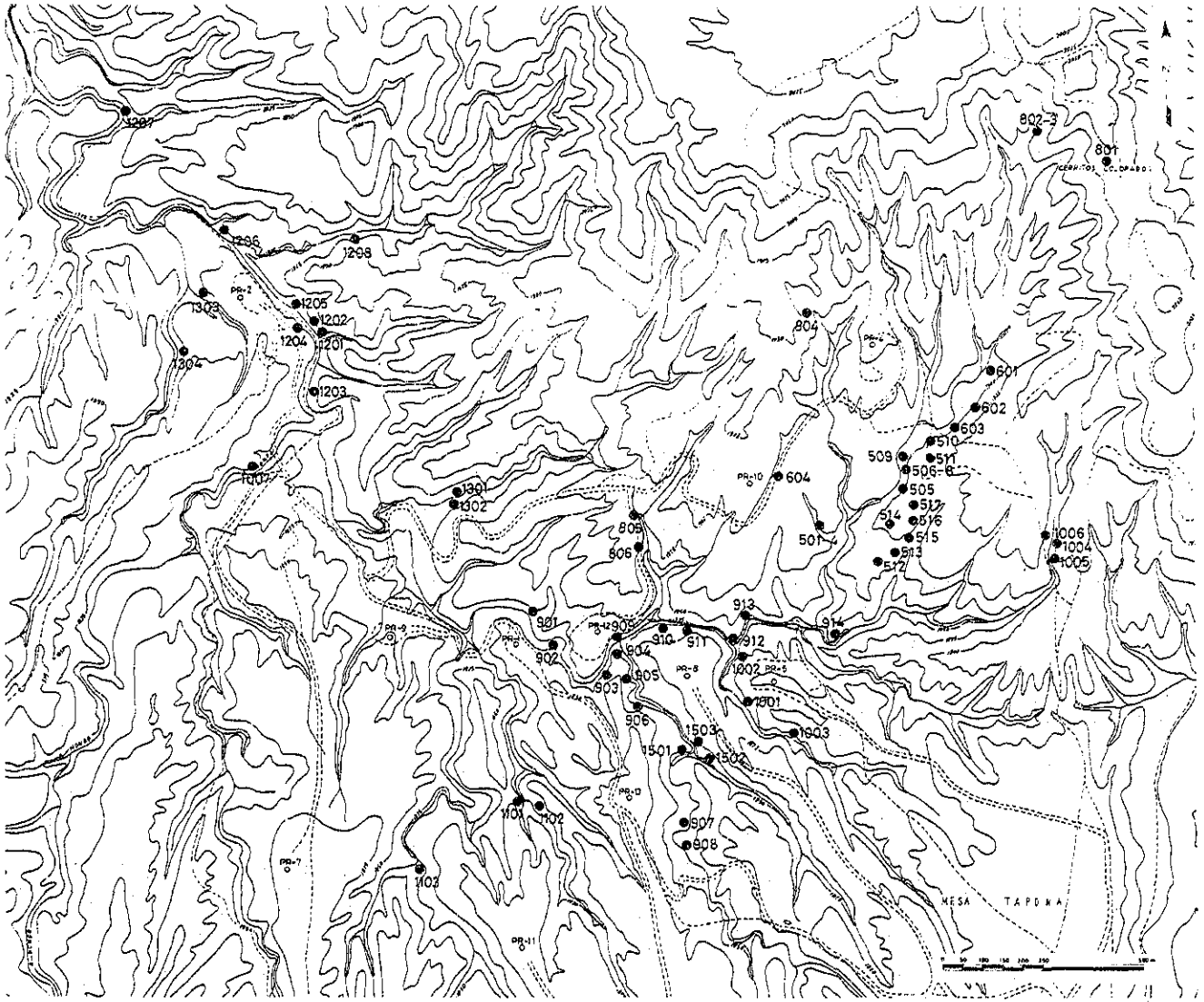

Fig. II. 1-12 Locality Map of Surface Altered Rocks for X-Ray

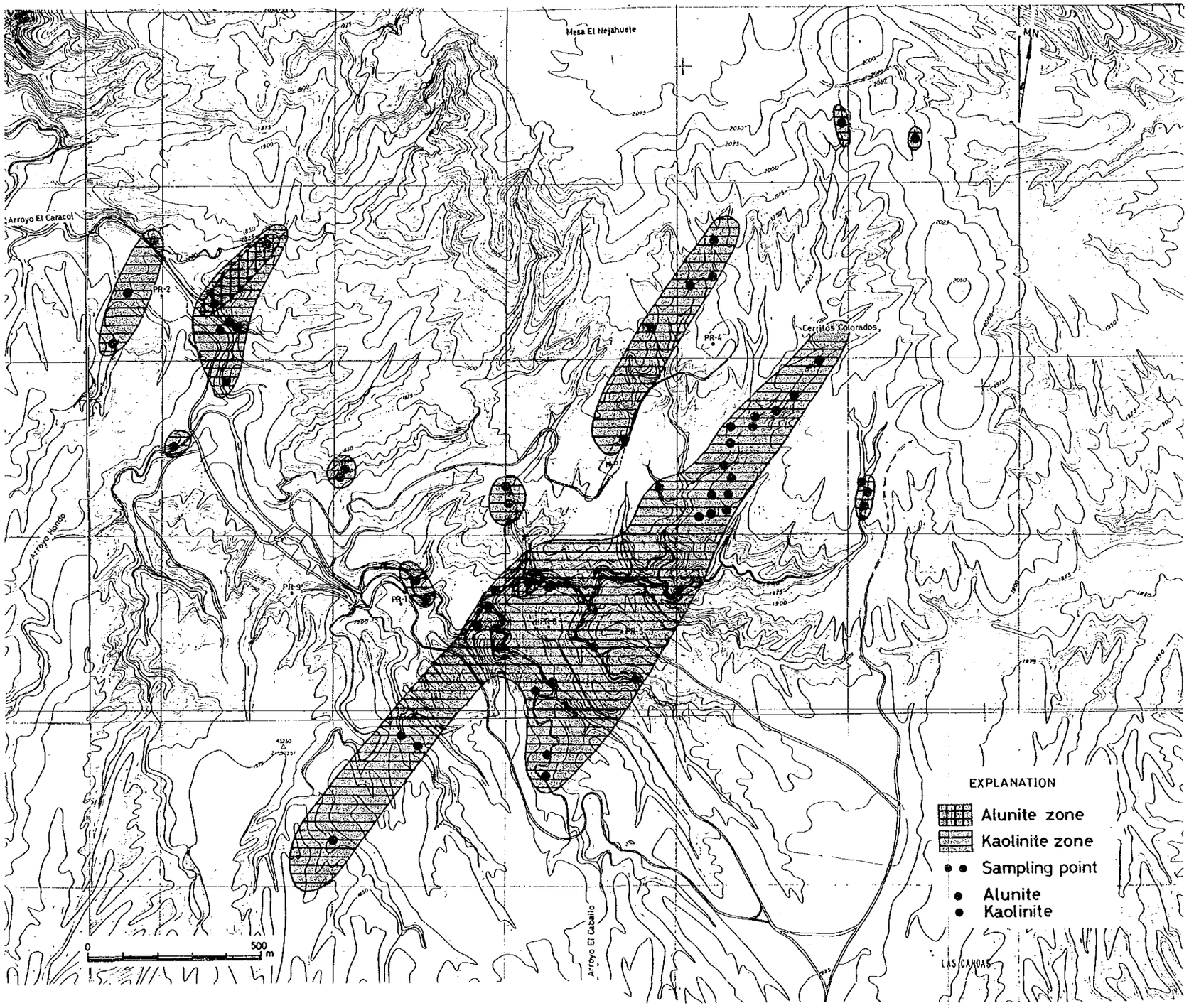

Fig. II. 1-13 Zoning Map of Rock Alternation

Table II. 1-4 Relationship Between Conjugate Minor Fault and Principal Stress at each Survey Point

Loc. No.	Conjugate Set		Principal Stress			Shear Angle (2θ)	Remarks
			σ_1	σ_2	σ_3		
3	N20E, 68W	N7E , 77W	N30E, 70N	N11E, 19S	N77W, 6W	37	N with L
5	N18E, 78W	N2E , 76E	N8E , 60S	N11E, 31N	N80W, 1W	30	N with L
12	N37E, 76E	N30E, 62W	N2E , 79N	N34E, 9W	N57W, 7E	42	N
13	N30E, 85W	N42E, 83E	N37E, 43E	N35E, 47W	N55W, 1W	18	L with N
15	N31E, 80E	N70E, 72N	N55E, 36W	N44E, 54E	N40W, 5E	46	L with N
22	N40W, 58E	N40W, 77W	N50E, 80E	N40W, 0	N50E, 10W	45	N
27	N32E, 76E	N40E, 82W	N34E, 64W	N38E, 26E	N53W, 2W	23	N with L
28	N24E, 78W	N25E, 75E	N68E, 87E	N24E, 2S	N66W, 2W	26	N
30	N10W, 68E	N4E , 72W	N6W , 68S	N2W , 22N	N88E, 2W	44	N with L
31	N38E, 70E	N20E, 68W	N28E, 68N	N29E, 22S	N62W, 1E	46	N with L
32	N6W , 74W	N10E, 71E	N7E , 66N	N1E , 23S	N88W, 2W	38	N with L
33	N20E, 77W	N24E, 82E	N46E, 82W	N25E, 8N	N65W, 3E	22	N
34	N39E, 60W	N54E, 80E	N22E, 67N	N50E, 20W	N44W, 10E	42	N with L
35	N63E, 61N	N33E, 85E	N64E, 47W	N37E, 39E	N42W, 14E	47	Oblique
36	N46E, 41E	N11E, 69W	N59E, 64E	N21E, 21S	N64W, 16W	40	N with L
38a	N22E, 62W	N20E, 82E	N87W, 80W	N20E, 3N	N69W, 10E	36	N
39	N43W, 63W	N49W, 77E	NS , 80S	N47W, 8W	N43E, 7E	40	N
40	N14W, 64E	N6W , 74W	N36W, 79E	N9W, 10N	N80E, 5W	43	N
41	N43E, 72E	N27E, 79W	N41E, 60E	N33E, 29W	N55W, 4W	32	N with L
44	N55E, 70E	N36E, 68W	N43E, 68E	N46E, 22W	N45W, 1E	46	N with L
47	N6E , 75E	N52E, 59W	N38E, 46W	N20E, 43N	N63W, 8E	64	Oblique
48	N20E, 65E	N25E, 83W	N25W, 75S	N24E, 10N	N68W, 10W	32	N
50	N45E, 87W	N36E, 78E	N34E, 56W	N43E, 34E	N50W, 4W	18	Oblique
56	N10E, 73W	N62E, 75S	N37E, 34E	N39E, 56W	N54W, 0	54	L with N
59	N22W, 58W	N20W, 60E	N56W, 87W	N21W, 2E	N68E, 2S	62	N
61	N36E, 65W	N10E, 68E	N27E, 62S	N22E, 28N	N68W, 2E	52	N with L
62	N26W, 67W	N26W, 62E	N65E, 87E	N26W, 0	N65E, 3W	50	N
64	N31E, 57E	N28E, 52W	N25W, 86N	N29E, 2S	N61W, 3E	70	N
68	N11W, 77W	N28W, 87E	N16W, 42S	N26W, 47N	N70E, 5E	25	Oblique
69	N11E, 79W	N40W, 70E	N18W, 33S	N6W , 57N	N77E, 5W	56	Oblique
70	N33W, 62E	N47W, 79W	N13W, 70N	N42W, 18E	N50E, 10W	40	N
72	N35E, 67W	N25W, 70E	N6E , 37S	N2E , 51N	N86W, 2E	72	Oblique

Loc. No.	Conjugate Set		Principal Stress			Shear Angle (2θ)	Remarks
			σ_1	σ_2	σ_3		
73	N48W, 84E	NS , 56E	N13W, 40S	N41W, 45W	N63E, 15E	59	Oblique
79	N12E, 74W	N28E, 77E	N18E, 62N	N20E, 29S	N72W, 1E	33	N with L
83	N68E, 74W	N42E, 77E	N55E, 49W	N53E, 41E	N36W, 1E	38	Oblique
85	N18E, 70E	N38W, 64W	N13W, 41N	N6W , 48S	N80E, 3E	70	Oblique
86	N55W, 29S	N74E, 57N	N23E, 50N	N87E, 19W	N16W, 33S	90	Oblique
88a	N42E, 62W	N32E, 68E	N55E, 80W	N37E, 10E	N53W, 4E	51	N with L
88b	N49E, 67W	N47E, 58E	N10W, 84S	N58E, 2E	N42W, 5W	55	N
88c	N47E, 62E	N47E, 67W	N43W, 87E	0	N43W, 3W	51	N
88d	N29E, 66W	N40E, 63E	N40E, 78E	N34E, 11S	N54W, 2W	52	N with L
89	EW	N79W, 68N	N84W, 74W	N84W, 15E	N6E , 1S	42	N with L
90	N4W , 83W	N56W, 88E	N30W, 10S	N42W, 80W	N60E, 2E	53	L
94	N26W, 78W	N48W, 88E	N34W, 33E	N46W, 56W	N53E, 10E	25	L with N
97	N13E, 73E	N27E, 65W	N26E, 71S	N18E, 18N	N71W, 4E	44	N with L
103	N6W , 67E	N18E, 72E	N2E , 60S	N7E , 30N	N84W, 2W	47	N with L
104	N2E , 55W	N22E, 72E	N16W, 70N	N16E, 18S	N78W, 10E	56	N with L
108	N58E, 56W	N49E, 61E	N73E, 82W	N54E, 8E	N36W, 3E	64	N
112	N74E. 84N	N67E, 61E	N29E, 78S	N72E, 9E	N20W, 9N	41	N
115	N48W, 60E	N76W, 69W	N54W, 62W	N65W, 27E	N27E, 4S	57	Oblique
116	NS , 83E	N20W, 75W	N14W, 49N	N7W , 41S	N81E, 4E	30	Oblique

Remarks: N : Normal-slip fault, N with L: Normal-slip with lateral component
L : Lateral-slip fault, L with N: Lateral-slip with normal component
Oblique: Oblique fault

Table II. 1-5 Remnant Magnetization of Cores

	Well number Depth of core Rock name	Demagne-tization mT	Strength of magnetization KA/m x 10^{-3}	Declination of assumed north (Clockwise)	Strike, dip and slip direction of fracture	Principal stress axis
1	PR-1 93 m Welded tuff	0 10 20 30	2.25 2.25 2.21 2.00	259° 259 260 258	Vein N70°W 32° NE	σ_1: N82°E, 30°W σ_2: N82°E, 60°E σ_3: N8°E , 0°
2	PR-1 910 m Welded tuff	0 10 20 30	2.29 2.31 2.28 2.09	231° 230 228 230	Slicken-side N30°W 63°S 80°	σ_1: N56°E, 84°W σ_2: N22°E, 5°NE σ_3: N69°W, 3°E
3	PR-1 915 m Welded tuff	0 10 20 30	1.49 1.52 1.50 1.43	170° 170 169 168	slicken-side 84°W 64°N 87°	σ_1: N60°E, 86°W σ_2: N11°W, 2°N σ_3: N78°E, 3°E
4	PR-2 350 m Welded tuff	0 10 20 30	2.95 2.90 2.21 1.22	108° 107 108 109	Slicken-side N40°W 30°N 90°	σ_1: N19°W, 60°S σ_2: N71°E, 0° σ_3: N19°W, 30°N
5	PR-2 1,360 m Andesite	0 10 20 30	7.47 6.86 5.43 3.49	61° 59 65 70	Vein S37°W 90° lateral separation is N53°E	σ_1: N81°W, 38°E σ_2: N46°E, 38°SW σ_3: N18°W, 29°N
6	PR-4 300 m Welded tuff	0 10 20 30	4.17 3.51 2.86 2.26	19° 19 18 17	Vein N10°E 85°SE	σ_1: N58°W, 85°E σ_2: N63°E, 5°W σ_3: N27°E, 0°
7	PR-5 350 m Welded tuff	0 10 20 30	4.17 3.43 2.58 2.07	85° 88 88 85	Slicken-side NS 80°E 90°	σ_1: N 5°W, 70°N σ_2: N85°E, 0° σ_3: N 5°W, 20°S
8	RC-1 700 m Andesite	0 10 20 30	9.24 9.18 8.63 7.12	198° 198 199 198	Slicken-side N37°W 54°S 60°	σ_1: N36°W, 74°S σ_2: N 8°W, 15°N σ_3: N81°E, 3°W

Table II. 1-6 Result of X-Ray Analysis for Surface Altered Rock

No.	Mineral / Sample No.	Plagioclase	K-feldspar (Sanidine)	Quartz	Cristobalite	Tridymite	Calcite	Sulfur	Alunogen		Montmorillonite	Chlorite/Montmorillonite	Sericite/Montmorillonite	Sericite		Kaolin	Halloysite	Gibbsite	Alunite		Pyrite	Amorphous silica
		Pl	Kf	Qt	Cb	Td					Mt	Ch/Mt	Se/Mt	Se		Kn	Ha		An		Py	
1	501		○													○						
2	502															○						
3	503		○													○						
4	504		○	○							●					○						
5	505		○		○											○						
6	506		○		○											○	○					
7	507		○		◎	◎										○					●	
8	508		○		◎											○						
9	509		○	●	◎											○						
10	510															◎						
11	511		○	●	●											○	●					
12	512			○												○						
13	513			○	○	●										○						
14	514			○	●											◎						
15	515			●	●											○						
16	516				●											○						
17	517															○						
18	601		●		○											○						
19	602		○		◎	○										○					●	
20	603		○													○						
21	604		○		○											○						
22	801		○	○												○	○					
23	802		●	○										●		○						
24	803		●	●												○	○					
25	804	●	●	◎												○					●	
26	805		○	○												○						
27	806		○	○	○											○	○				●	
28	901			●												○						
29	902a			○	○									●		○					●	
30	902b		○	●	○									●		○						
31	903		●													○						

No.	Mineral / Sample No.	Plagioclase	K-feldspar (Sanidine)	Quartz	Cristobalite	Tridymite	Calcite	Sulfur	Alunogen		Montmorillonite	Chlorite/Montmorillonite	Sericite/Montmorillonite	Sericite		Kaolin	Halloysite	Gibbsite	Alunite		Pyrite	Amorphous silica
		Pl	Kf	Qt	Cb	Td					Mt	Ch/Mt	Se/Mt	Se		Kn	Ha		An		Py	
32	904			●												○						
33	905		○		◎	◎										○						
34	906a															◎						
35	906b			●	●											○						
36	906c															○					○	
37	907		○													○						
38	908		○													○						
39	909a		○	○												○						
40	909b																					○
41	910			●	●											◎			○			
42	911															◎					●	
43	912			○												○						
44	913		○													○						
45	914		○	●												○						
46	1001		○	○	○											○						
47	1002a		○	●												○						
48	1002b		○													○						
49	1003		○	◎												○						
50	1004															○					●	
51	1005		○		○											◎						
52	1006																					
53	1007		○		◎											○					●	
54	1101a															◎						
55	1101b			○												○						
56	1102		○	○												○						
57	1103a		○	●												●						
58	1103b		○													○						
59	1103c															○						
60	1201																					
61	1202		○		◎																	
62	1203		○	○	●											○						

No.	Mineral / Sample No.	Plagioclase	K-feldspar (Sanidine)	Quartz	Cristobalite	Tridymite	Calcite	Sulfur	Alunogen		Montmorillonite	Chlorite/Montmorillonite	Sericite/Montmorillonite	Sericite		Kaolin	Halloysite	Gibbsite	Alunite		Pyrite	Amorphous silica
		Pl	Kf	Qt	Cb	Td					Mt	Ch/Mt	Se/Mt	Se		Kn	Ha		An		Py	
63	1204		○		◎											○						
64	1205a		○			◎										○						
65	1205b					○		○											◎			
66	1205c				◎											○			○			
67	1205d		○		◎											●						
68	1205e				◎																	
69	1206		○			◎										○						
70	1207																					
71	1208a					○	○		○							○			◎			
72	1208b					○			◎							○		○	○			
73	1301		●	○	●											○						
74	1302		○	○												○						
75	1303			●												○						
76	1304		○	○	●											○						
77	1501		○	●	●											○						
78	1502															◎						
79	1503		○													○						
80	2001		○		◎											○						
81	2002				●											○						
82	2003		○	●	○											○	○					

◎ Abundant (scale out of maximum peak)
○ Medium (from 4 cm to full scale of maximum peak)
○ Little (from 2 cm to 4 cm of maximum peak)
● Rare (under 2 cm of maximum peak)

Table II. 1-7 Result of Density, Effective Porosity and Conductivity of Core Samples

No.	Well	Sampling depth (m)	Rock name	Density of rock (g/cm³)			Effective porosity	Conductivity
				Natural water	Dry condition	Wet condition	(%)	(10^{-3} cal/ cm·sec·°C)
1	PR-1	93	welded tuff	2.00	1.98	2.17	19.2	3.0625 ± 0.0380
2	PR-1	911 ~ 912	welded tuff	1.92	1.91	2.12	21.1	2.612 ± 0.0167
3	PR-2	350 ~ 352	welded tuff	2.31	2.30	2.34	3.6	4.851 ± 0.0483
4	PR-2	668 ~ 672	lapilli tuff	1.71	1.65	1.84	19.4	1.5375 ± 0.0200
5	PR-2	901 ~ 902	welded tuff	1.96	1.86	2.12	25.8	2.1223 ± 0.0164
6	PR-2	1,360 ~ 1,361	andesite	2.16	2.11	2.26	14.7	3.282 ± 0.0663
7	PR-4	300 ~ 301	welded tuff	2.24	2.22	2.30	8.3	4.256 ± 0.0204
8	PR-5	200 ~ 202	welded tuff	2.23	2.21	2.26	5.1	4.464 ± 0.0297
9	PR-5	430 ~ 431.5	welded tuff	2.19	2.17	2.21	3.2	4.1542 ± 0.0489
10	RC-1	700 ~ 702	andesite	2.17	2.00	2.23	23.1	2.573 ± 0.0513
11	RC-1	1,189 ~ 1,190	basaltic andesite	2.49	2.41	2.54	12.4	3.289 ± 0.0470
12	RC-1	1,500 ~ 1,503	andesite	2.25	2.14	2.28	14.8	3.218 ± 0.0332

PR-9 (2,985.00 m ~ 2,986.00 m)

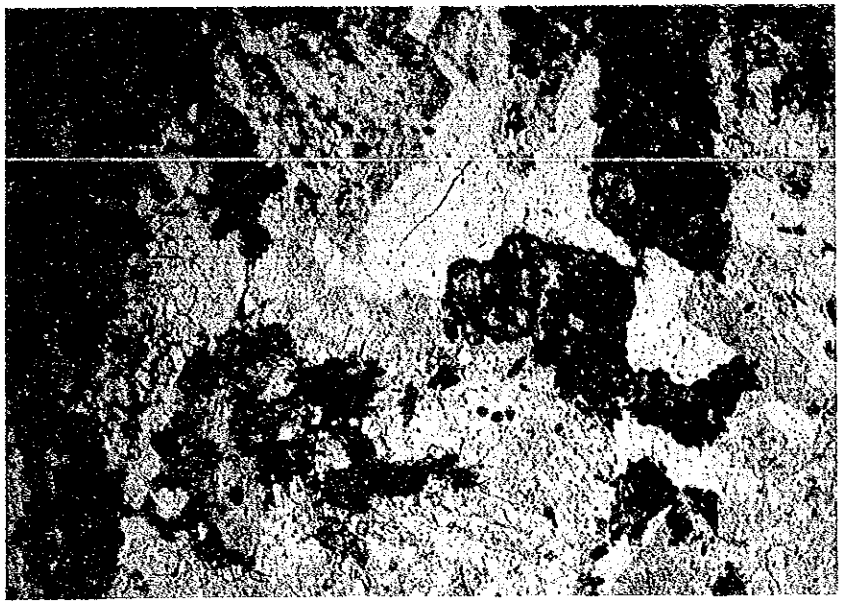

Open nicol

0 0.5 mm

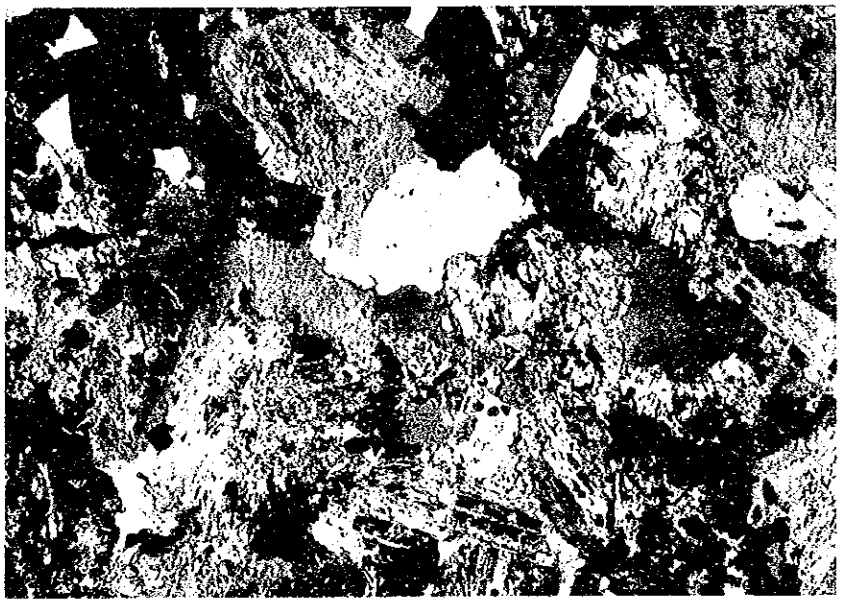

Crossed nicols

0 0.5 mm

Photo 1 Microscopic Photos of Biotite Granite

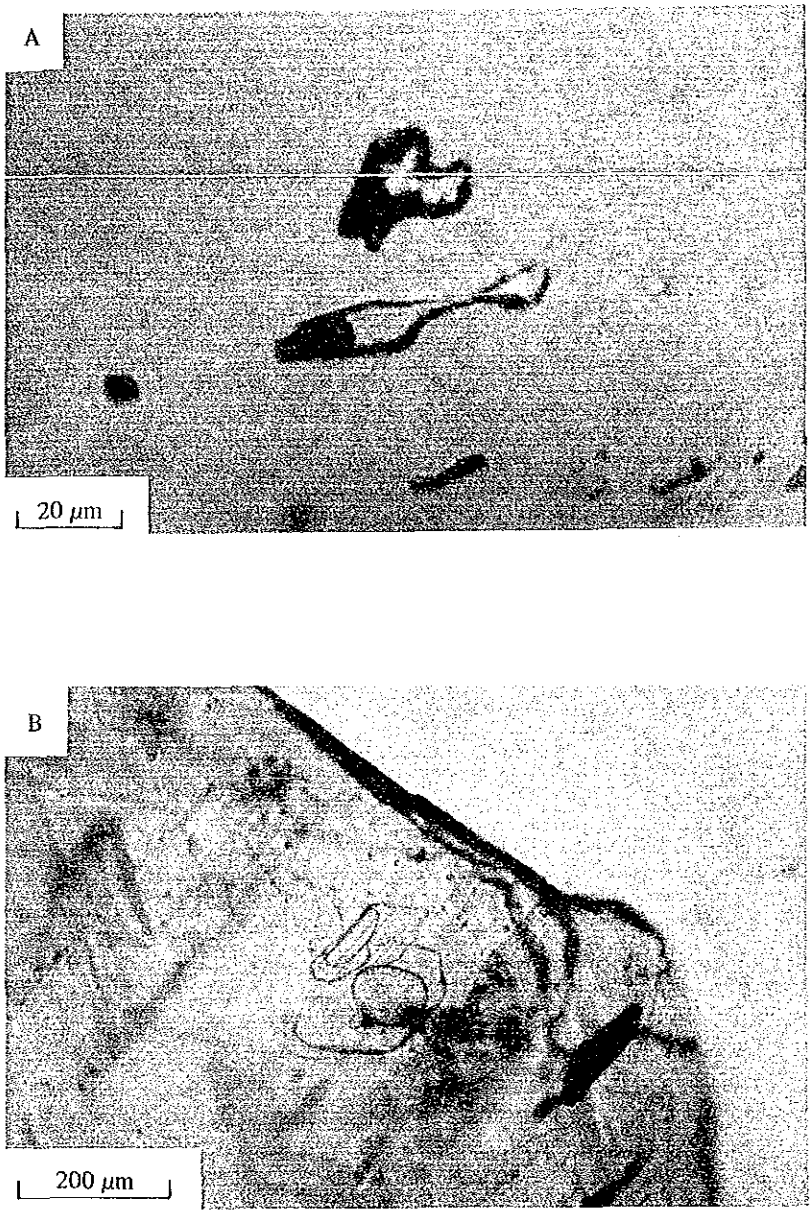

Photo 2 A: Liquid Inclusion in Vein Quartz from the Core of PR-13 (Depth: 2,004 m)
B: Liquid Inclusion in Vein Ankerite from the Cuttings of PR-10 (Depth: 1,720 m)

1.2 Geochemical survey

1.2.1 Summary of geochemical survey

To estimate the extent of geothermal activity and to determine the circulating mechanism of geothermal fluid flows, two geochemical surveys were carried out on the mercury concentration analysis and the chemical analysis of wellbore fluids which emit from the wells drilled by CFE. Moreover, an attempt was made to the estimate fractures and temperature based on the geochemical study.

The first geochemical survey was the mercury concentration analysis in soil of 272 points. The second geochemical survey was the chemical analysis of geothermal fluids from PR-1 and PR-8.

The following are results of the geochemical survey in this area:

① The mercury concentration can be divided into two groups with the boundary of 70 ppb. The high mercury concentration of more than 70 ppb is distributed in the east of the surveyed area having the NE-SW trend. This fact means that the NE-SW trending fractures are existing in the subsurface of the high mercury concentration area, that is, the NE-SW trending faults in the geological map (fig. II.1-1). Thus, the high mercury concentration in soil signifies the accumulation of mercury provided from the subsurface fluids in volcanic origin up to the present.

② The investigation into the chemical geothermometer of PR-1 and PR-8 finds the value of Na-K-Ca thermometer appropriate, and estimates about 300°C for PR-1 and about 280°C for PR-8.

③ Considering the relation of the enthalpy and B with Cl-concentration, the deep-seated geothermal hot water originates in the deep formation near PR-1 and flows toward PR-8 and PR-5. Furthermore, the hot water flow toward PR-4 along the NE-SW trending fractures are being influenced by mixing of surface water gradually.

The fact that hot water from PR-1 is in close association with the deep-seated essential hot water, is supported by the high value of $\delta^{18}O$ in isotopic composition and the high ratio of He/Ar in gas.

1.2.2 Mercury concentration survey in soil

Two hundred and sevently two points for the mercury survey were set up within a network of the extent of 9.6 km^2 with borderlines of 3.2 km length to E-W and of 3 km to N-S, enclosing the geothermal manifestation area at the center (Fig. II.1-14). The soil samples were taken from holes which are bored 1 meter deep by using hand-auger at the intersection points of a network, avoiding the construction, steep slop and river. The air dried samples were crushed into powder under 200 mesh, and were analyzed by the mercury detector made in Rigaku of atomic absorption method. The results of mercury analysis are listed in Table II-1.8.

At first, a distribution histogram (Fig. II.1-15) and a cumulative frequency (Fig. II.1-16) of mercury concentration were prepared on the basis of the results. Fig. II.1-16 shows that the mercury concentration can be divided into two groups with a boundary of 70 ppb and is inferred to be two mechanisms for the mercury rising. Of these mechanisms, the

higher concentration of mercury would be resulted from the ascent through fractures, while the lower one shows a gradual accumulation through the pores in the formation. The mercury concentration is subdivided into five grades with the boundaries of 18, 32, 70 and 178 ppb to make a distribution map of mercury shown in Fig. II.1-17. Fig. II.1-17 indicates that the points of higher condentration more than 70 ppb are located in the east of the surveyed area and several zones of crowded high concentration are observed.

Secondly, the third-order trend surface analysis was tried for the values of mercury concentration in order to examine the orientation of concentration. Fig. II.1-18 shows the result of trend surface analysis. The high concentration has a line arrangement with a NE-SW orientation. That is to say, both distribution of high mercury concentration and that of natural fumarole show a similar NE-SW trend with overlapping location in the east of this area. Consequently, it would be presumed that the NE-SW trending fractures, which provide high mercury concentration and natural fumarole, exist in this area.

On the other hand, fumarole and high mercury concentration surrounding PR-2 show a discontinuous and isolated distribution compared with that of the east, resulting in no presence of fracture in large scale around PR-2.

1.2.3 Chemical analysis of wellbore fluids

Steam, condensed water and hot water from PR-1 and PR-8 were chemically analyzed, followed by a consideration on the geothermal reservoir mechanism based on their chemical characteristics. The collecting method, the analytical method and the result of chemical composition are given in Fig. II.1-19 and Tables II.1-9~10 respectively. An attempt has been made on the following investigations on the basis of the result of chemical composition:

(1) Chemical geothermometer

For the purpose of estimating fluid temperature, four types of chemical geothermometers were investigated. They are the solubility of Quartz (adiabatic cooling), two types of Na/K ratio proposed separately by two authors and Na/K ratio corrected by Ca (Table II.1-11). The values from these four geothermometers were nearly the same for PR-1, whereas those for PR-8 showed remarkable dispersion. Taking into account that the reaction rate of Quartz dissolution increases above 250°C and the re-equilibrium takes place during fluid flow-up in the borehole, the fluid temperature in PR-8 might be more than 274°C. The value of Na-K-Ca geothermometer, therefore, seems to be adequate.

The downhole temperature measurements record 299°C at 1,800 m for PR-1 and 235°C at 1,800 m for PR-8. The fluids are flowing up under two-phase condition after flashing in the formation in both wells, but a certain water level was confirmed near the bottom of PR-1. The difference between the value of downhole temperature and that of chemical geothermometer seems to be caused by the flashing in the formation.

(2) Relationship between enthalpy and chloride concentration

The relation of enthalpy with chloride concentration (Cl^- value is flash-corrected by Na-K-Ca thermometer) in deep hot water was studied to estimate the flow conditions of

geothermal fluids in the underground. (Fig. II.1-20). As shown in Fig. II.1-20, the values on PR-1, 4.5 and 8 are standing on a straight line. Among these values, the values of PR-2, 4 and 5 were given by the data from CFE. The placing in a line suggests that the hot water originated in the deep formation near PR-1 and is contaminated with the surface water through flowing from PR-1 to PR-8 and PR-5. The enthalpy and Cl^--concentration of the surface water are low, so that PR-4, of which depth is less than 600 m, can be strongly influenced by the mixing of the surface water. Moreover, the fluid flow mechanism from PR-8 and PR-5 to PR-4 is supported by the existence of fractures having NE-SW trend which was confirmed by a soil mercury servey and geological survey.

Chemical characteristics of hot water in PR-2 are different from those in other wells as shown in Fig. II.1-20. Thus, an independent hot water reservoir might exist in case of PR-2 since the results of soil mercury survey show no existence of high concentration area between PR-2 and other wells.

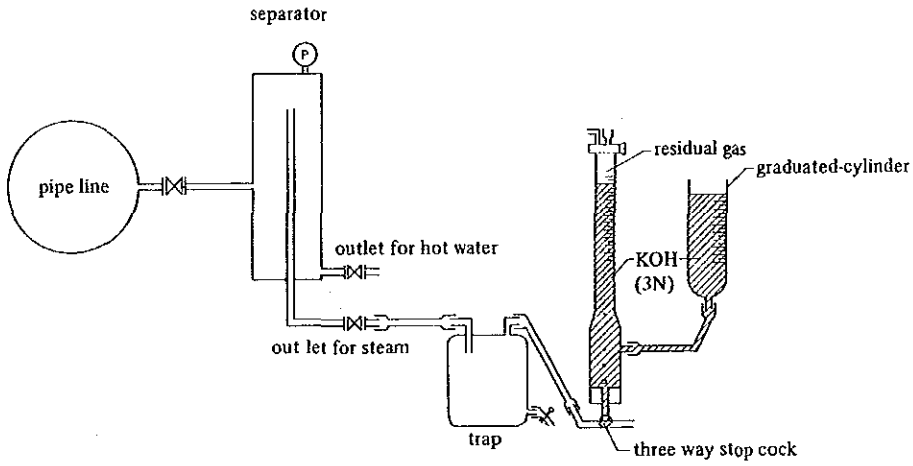

Fig. II. 1-19 Apparatus for Collecting of Steam Sample

Table II. 1-11 Chemical Geothermometer

Geothermometer			(°C)	
Well	Quartz-maximum steam loss	Na/K (Fournier)	Na/K (Truesdell)	Na-K-Ca
PR-1	> 288	301	299	297
PR-8	> 274	263	247	280

(3) Relationship between Boron and Chloride concentrations

Fig. II-1-21 shows the relation between B and Cl concentrations in deep hot water of PR-1, 2, 4, 5 and 8. In general, the high ratio of B/Cl indicates a vapor dominated reservoir (ex. Matsukawa in Fig. II.1-21), while the low ratio of B/Cl shows a brine reservoir (ex. Cerro Prieto in Fig. II.1-21). The ratio of B/Cl obtained from the wells in this area is centralized about 0.1. It means that the geothermal fluids are provided from the same reservoir in chemical characteristics.

Because low chloride concentration in Fig. II.1-21 indicates the degree of dilution by fresh water, the order from PR-1 to PR-4 expresses the increasing dilution. The ratio of B/Cl in PR-2 differs from that of other wells, and is concordant with the relation between the enthelpy and the chloride concentration.

(4) Gaseous component in steam

A verification was made on He, Ar and N_2 in steam. Fig. II.1-22 shows that nearly the same ratios of He/Ar and N_2/Ar were obtained from steam of PR-1 and PR-8. In Fig. II.1-22, (He/Ar)s/(He/Ar) air and (N_2/Ar)s/(N_2/Ar) air are normalized by utilizing the atmospheric values to ratios of He/Ar and N_2/Ar in the sample. The value from Hervores de la Vega, a hot spring in the neighborhood, is close to the mixing line which is drawn by the values of PR-1 and PR-8 and by the value of the surface water balancing with the atmosphere (points marked with "diss, air" in Fig. II.1-22).

Therefore, the deep gas in this area, after mixing with the atmosphere dissolved in the surface water in various ratios, is discharged as the geothermal gas in steam. The gas from the wells of La Primavera is considered to be closer to the deep gas compared with the hot spring gas.

(5) Isotopic composition

An isotopic composition diagram was prepared to study the origin of water and its fluid flow mechanism as shown in Fig. II.1-23. A straight line in this diagram shows the value of the surface water expressed by an equation $\delta D = 8 \times \delta^{18}O + 10$ (Craig, 1961). In addition to the isotopic composition of hot water from PR-1 and PR-8, the values of hot spring water, which were given by the analysis of CFE, are dotted in this diagram. The $\delta^{18}O$ values of PR-1 and PR-8, in particular of PR-1, indicate high values. It would be attributed to the "Oxygen Shift" which makes a high $\delta^{18}O$ value of hot water due to an oxygen isotope exchange with rock. From this fact it is concluded that the hot water of PR-1 has close characteristics with deep-seated hot water compared with that of PR-8.

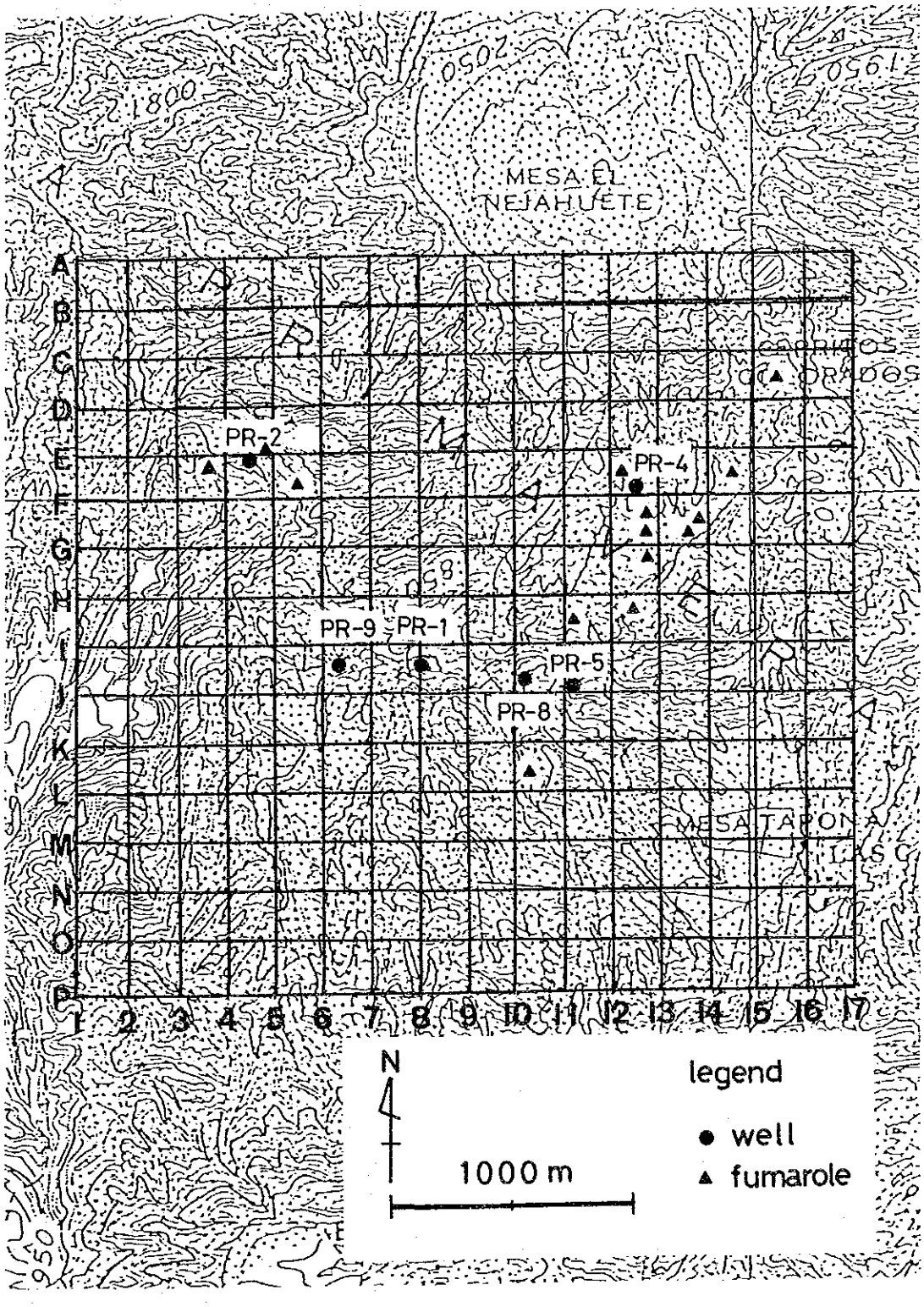

Fig. II. 1-14 Location Map of Soil Mercury Survey

Table II. 1-8 Mercury Concentration Value in Soil

(ppb)

	1	2	3	4	5	6	7	8	9	10	11	12	13	14	15	16	17
A	35.8	20.5	19.9	19.2	20.0	27.7	11.3	34.8	32.8	39.4	26.4	24.9	18.1	35.1	13.9	34.9	32.6
B	15.2	14.2	10.5	7.0	31.6	21.7	20.1	34.1	87.1	21.4	30.5	22.3	23.8	16.8	123	429	18.1
C	24.2	14.6	16.3	36.6	17.5	21.0	22.1	19.4	24.5	31.8	16.3	13.0	35.1	19.7	37.0	32.0	16.4
D	21.7	22.4	53.1	66.5	12.8	18.0	24.6	14.7	24.7	24.7	23.2	15.8	73.0	10.6	34.3	51.8	29.9
E	32.5	10.6	22.6	60.8	919	19.6	49.6	12.2	32.3	40.1	57.9	10.4	8.7	16.9	36.8	24.2	22.5
F	33.0	23.3	43.9	29.8	15.5	19.6	32.8	43.2	33.2	28.0	31.3	6.0	15.3	27.7	30.0	41.7	9.9
G	39.4	32.1	63.8	32.0	58.4	12.0	17.3	11.2	16.5	23.2	23.7	565	15.3	10.7	32.1	15.6	17.9
H	34.9	38.6	22.1	61.7	17.8	22.3	9.2	11.7	19.7	8.3	58.0	311	1405	45.6	36.2	16.7	111
I	38.3	26.4	48.9	39.4	29.6	31.1	26.5	42.5	32.7	23.6	24.3	72.6	19.5	22.1	71.4	38.2	55.8
J	48.9	38.3	87.8	22.9	26.2	28.9	21.7	18.0	14.6	31.5	16.8	40.5	10.9	11.1	22.2	30.0	12.4
K	62.9	45.2	52.6	39.5	39.3	50.0	21.4	13.4	48.3	46.0	32.9	26.4	68.5	66.9	40.8	16.3	22.4
L	16.6	11.1	37.4	51.0	43.2	44.8	39.8	29.7	74.4	221	38.6	36.6	42.0	58.7	29.7	23.0	21.2
M	21.1	27.5	43.7	26.0	23.5	11.3	20.2	42.7	34.6	33.7	8.0	25.6	25.3	37.8	34.4	11.1	9.6
N	8.5	19.2	26.3	21.2	28.6	14.5	70.2	31.1	48.8	39.2	37.1	31.0	32.6	30.5	21.6	6.7	13.8
O	16.1	28.0	33.7	8.1	15.1	43.5	16.9	23.7	21.0	20.6	19.5	57.1	30.7	23.4	17.9	12.9	15.3
P	19.1	30.0	40.1	41.6	17.7	45.5	20.7	33.5	18.0	20.5	22.8	52.7	39.5	19.0	16.5	10.8	11.9

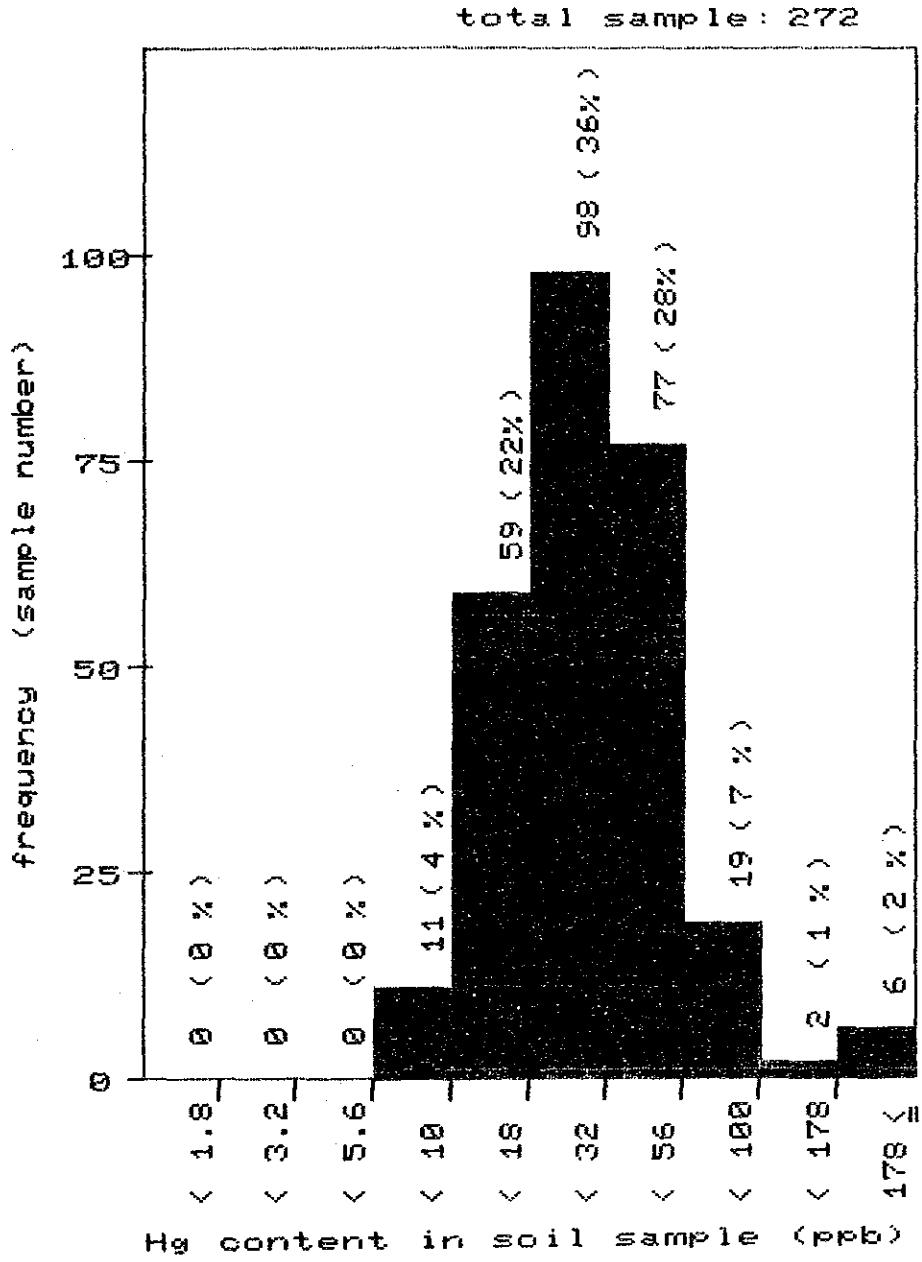

Fig. II. 1-15 *Distribution Histogram for Mercury Concentration in Soil Sample*

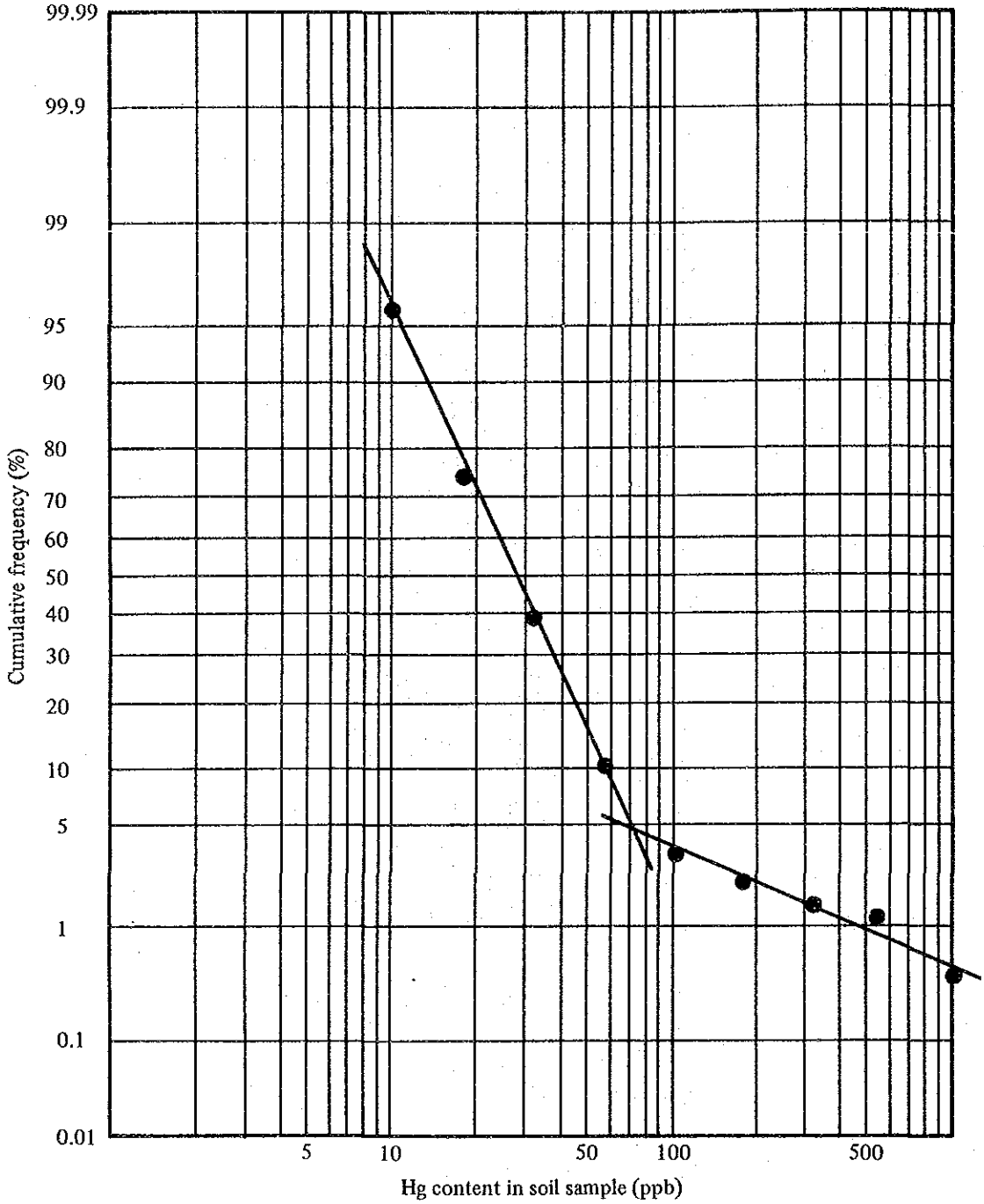

Fig. II. 1-16 Cumulative Frequency of Mercury Concentration in Soil Sample

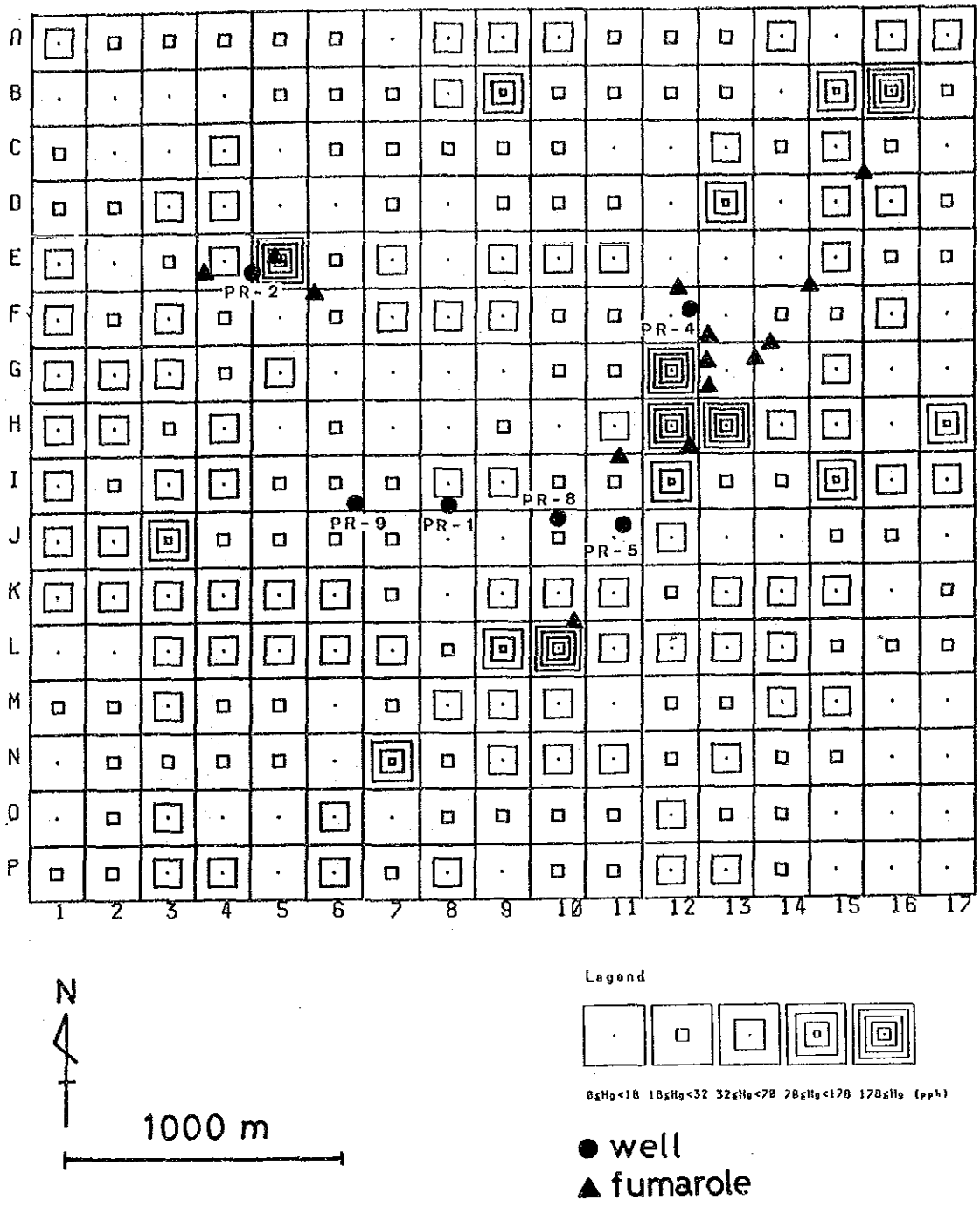

Fig. II. 1-17 Distribution Map of Hg Concentration in Soil

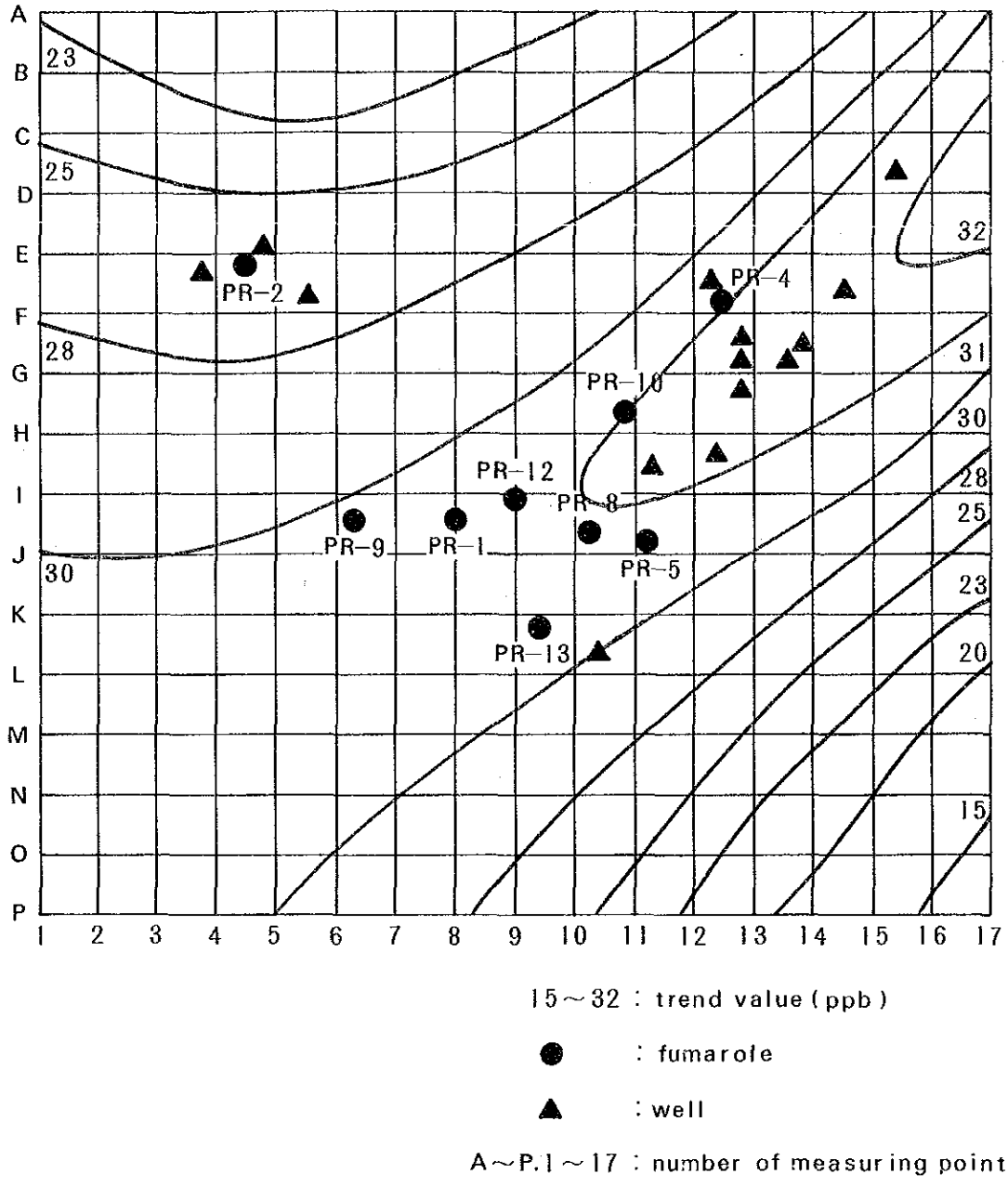

Fig. II. 1-18 **Result of the Third-order Trend Surface Analysis for Mercury Concentration Value**

Table II. 1-9 Analytical Method of Hot Water and Steam Condensed Water

element	analytical method
pH	glass electrode method
Cl	Mohr's method (hot water)
	absorptiometric method (condensed water)
SO_4	gravimetric method
HCO_3	micro diffusion method
Na	flame photometry
K	flame photometry
Ca	atomic absorption method
Mg	atomic absorption method
Li	atomic absorption method
Hg	atomic absorption method
As	atomic absorption method
SiO_2	gravimetric method
Fe	absorptiometric method (Oxine/$CHCl_3$)
Al	absorptiometric method (Oxine/$CHCl_3$)
B	absorptiometric method (Methylene Blue)
F	absorptiometric method (La-Alizarin)
NH_4	absorptiometric method (Nessler's method)
δD	mass spectrometry
$\delta^{18}O$	mass spectrometry
Tritium	liquid scintillation method

Table II. 1-10 Chemical Composition of Well Discharge Sample

(a) Chemical composition of steam condensed water.

Component	Unit	PR-1	PR-8
Electrical conductivity	μS/cm	2360	3180
pH	–	4.90	6.00
Cl	mg/ℓ	0.06	667
NH_4	mg/ℓ	19.7	39.3
As	mg/ℓ	0.03	6.08
Hg	ng/ℓ	5.4	5.7

(b) Gas composition of steam.

		PR-1	PR-8
Liquid-vapor separate pressure		4.8 Kg/cm²G	7.7 Kg/cm²G
Total gas in steam (vol %)		2.20	3.46
Gas composition	H_2S (vol %)	0.7	0.1
	CO_2 (vol %)	98.6	98.9
	H_2 (ppm)	1860	3310
	N_2 (ppm)	1740	2160
	CH_4 (ppm)	3360	4480
	He (ppm)	11.9	14.9
	Ar (ppm)	25.2	29.5

(c) Chemical composition of hot water.

Component	Unit	PR-1	PR-8
Electrical conductivity	μS/cm	4060	4340
Total dissolved solids	mg/ℓ	3830	3670
pH	–	7.80	8.60
Cl	mg/ℓ	1160	929
SO_4	mg/ℓ	44.4	109
H_2CO_3	mg/ℓ	2.7	1.4
HCO_3^-	mg/ℓ	71.2	227
CO_3^{2-}	mg/ℓ	0.3	6.9
Na	mg/ℓ	751	834
K	mg/ℓ	173	136
Ca	mg/ℓ	2.07	1.07
Mg	mg/ℓ	0.35	0.04
Fe	mg/ℓ	0.96	0.06
Al	mg/ℓ	1.25	0.08
SiO_2	mg/ℓ	1090	927
Li	mg/ℓ	6.52	6.40
B	mg/ℓ	174	125
F	mg/ℓ	8.4	7.9
NH_4	mg/ℓ	3.3	2.8
As	mg/ℓ	14.8	12.6
Hg	ng/ℓ	0.23	0.23
D/H	‰(SMOW)	−49.6	−57.0
$^{18}O/^{16}O$	‰(SMOW)	+0.7	−1.6
Tritium	T.U.	<0.23	<0.21

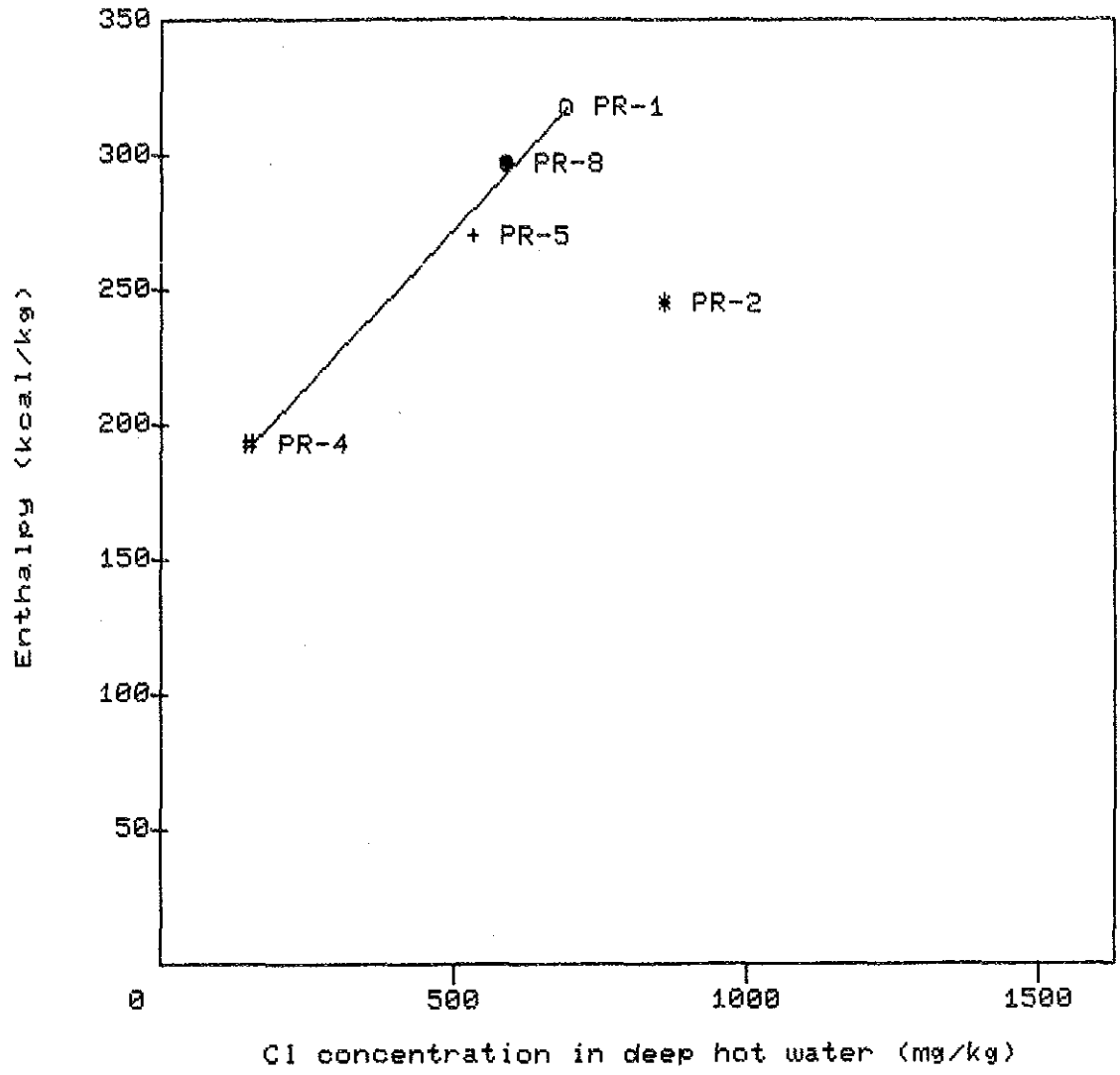

Fig. II. 1-20 **Relationship between Enthalpy and Chloride Concentration in Deep Hot Water in *the La Primavera***

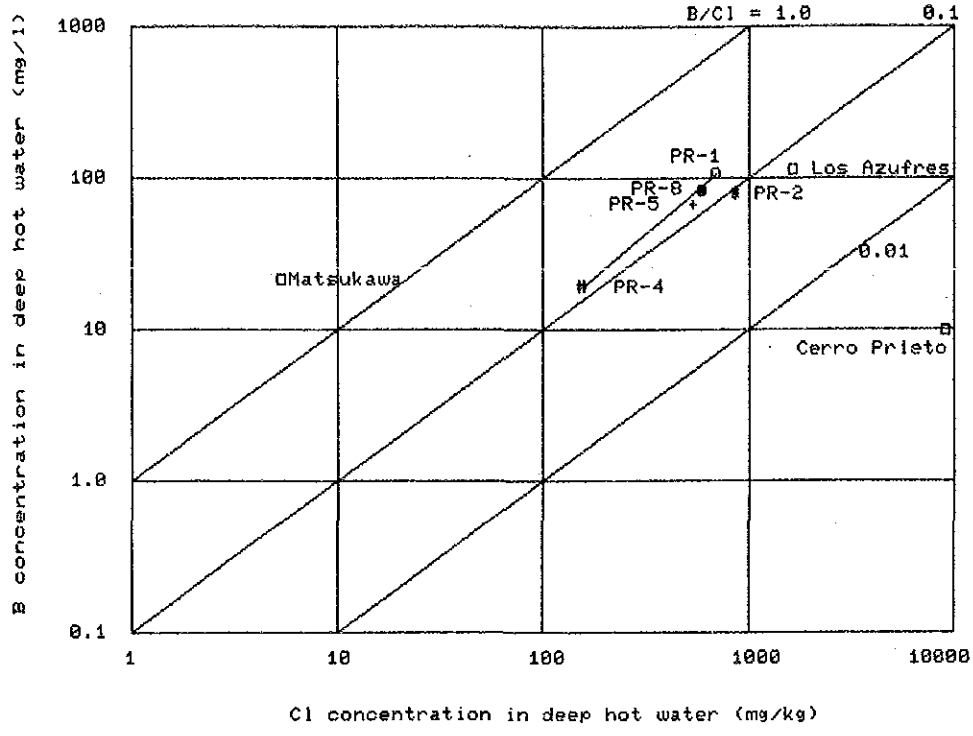

Fig. II. 1-21 Relationship between Boron and Chloride Concentration in Deep Hot Water

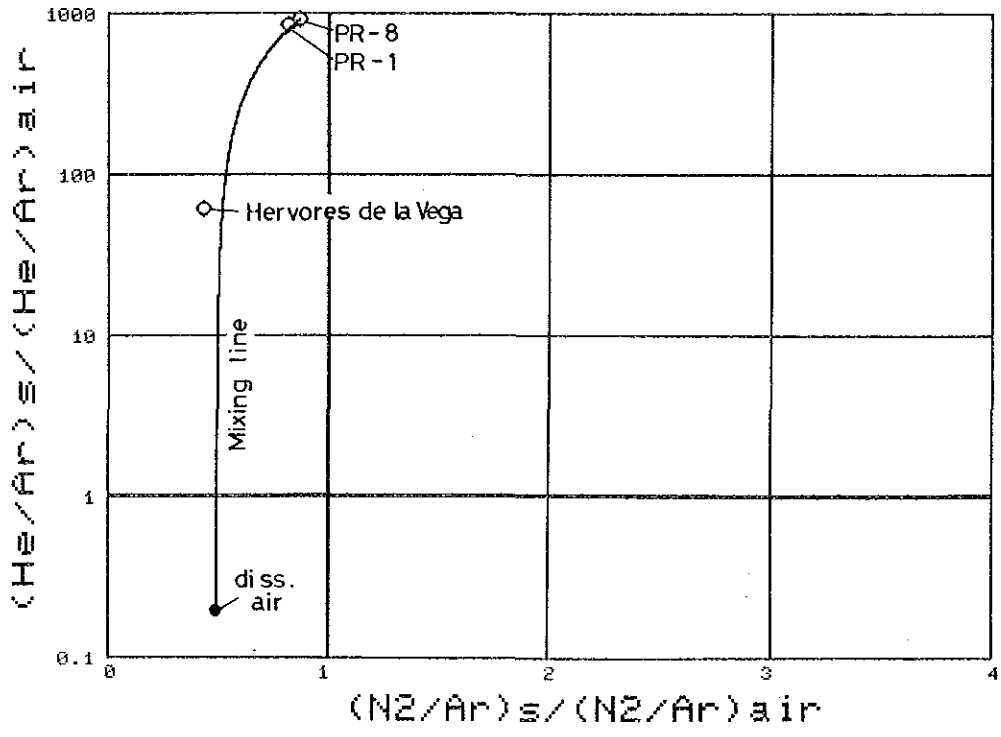

Fig. II. 1-22 Relationship between He/Ar and N_2/Ar Ratio in Geothermal Gaseous Discharge from PR-1 and PR-8

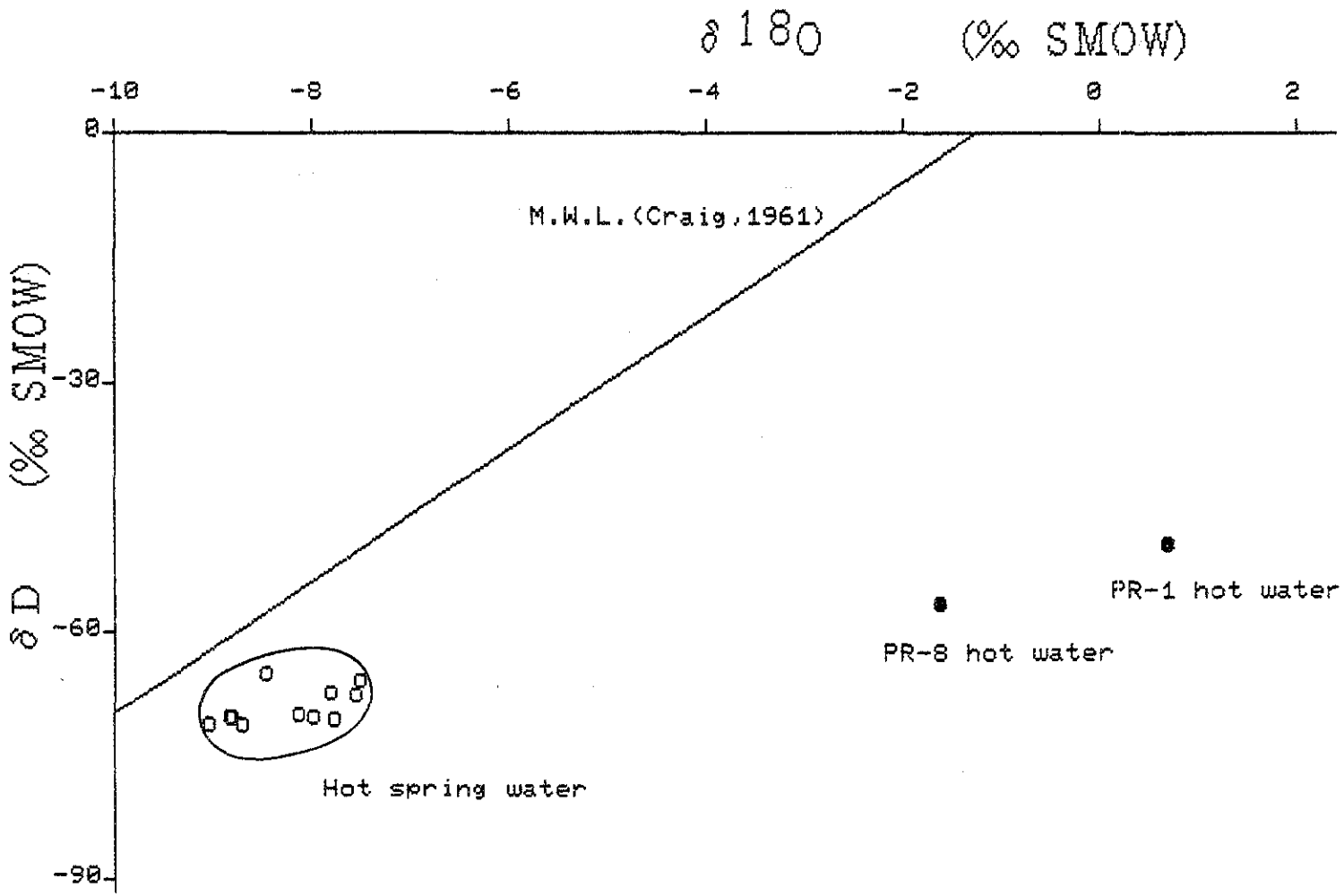

Fig. II. 1-23 Oxygen-18 and Deuterium Compositions of Hot Water of PR-1, PR-8 and Hot Springs and of Meteoric Waters